October 2020

STUDY OF CONTROL SCHEMES FOR SERIES HYBRID-ELECTRIC POWERTRAIN FOR UNMANNED AERIAL SYSTEMS

Darren A. Dehesa Jr
Louisiana State University at Baton Rouge

STUDY OF CONTROL SCHEMES FOR SERIES HYBRID-ELECTRIC POWERTRAIN FOR UNMANNED AERIAL SYSTEMS

A Thesis

Submitted to the Graduate Faculty of the
Louisiana State University and
Agricultural and Mechanical College
in partial fulfillment of the
requirements for the degree of
Master of Science

in

The Department of Mechanical and Industrial Engineering

by
Darren Anthony Dehesa, Jr.
B.S.M.E., Louisiana State University, 2018
December 2020

Acknowledgments

I would like to thank my major professor Dr. Shyam Menon and the rest of my committee, Dr. Ram Devireddy and Dr. Wanjun Wang. As an undergraduate, the thought of going to graduate school was full of uncertainty. However, after meeting with Dr. Menon and discussing the benefits of graduate school, I was excited to be returning to LSU to be a part of a new project on hybrid powertrains that he was beginning. Dr. Menon's dedication to graduate studies and his knowledge of hybrid powertrains was an invaluable quality that aided in completing my work. I would also like to thank the collaborative effort with James Benbrook and Dr. Chris Hagen from the Oregon State University as well as Kofi Agyemang Amankwah and Dr. Stephen Akwaboa from Southern University – Baton Rouge. Further, I would like to acknowledge the inputs and advice from Chad Miller, Dr. Michael Rottmayer, and Dr. Michael Rothenberger, and Dr. Thomas Howell at the Air Force Research Laboratory. I will always appreciate the warm welcome extended to me by everyone at AFRL during my stay over the summer.

Next, I would like to thank my fellow lab mates, who have been a tremendous help throughout my graduate career: Wanjun Dang, James Leung, Mohana Gurunadhan, and Varun Viswamithra. I will miss the conversation that we shared and the support that you gave. Also, I would like to thank the undergraduate researcher who helped get the hybrid testbed up and running: James Szeszycki and Matthew Monju. Your dedication and hard work with helping us assemble a functioning series hybrid testbed was very appreciated.

Lastly, I would like to thank my family and friends. If not for my parents, encouraging me to pursue my master's, I would not be where I am now. Without their love and support finishing these two years would have been difficult, and I'm grateful to have such a strong support group

pushing me to be the best that I can be. I'm incredibly grateful for the opportunities, knowledge, and experiences that I have gained over the years, and I will cherish them for times to come.

Table of Contents

List of Tables

List of Figures

Nomenclature

η	=	Efficiency
Q	=	Energy density
m	=	Mass
W	=	Weight
Ψ	=	Degree of hybridization
S	=	Power split
g	=	Acceleration due to gravity
L/D	=	Lift to drag ratio
E_{start}	=	Energy at takeoff
J	=	Motor inertia
L_i	=	Armature inductance
R	=	Armature resistance
b	=	Viscous damping friction
K_b	=	Back EMF constant
K_t	=	Motor torque constant
$\dot{\theta}$	=	Angular rotation
i	=	Current
V	=	Voltage
T	=	Torque
e	=	Back-EMF
C	=	C-Rate
OCV	=	Open circuit voltage

t = Time

τ = Time constant

J = Advance ratio

V_c = Flight speed

C_T = Thrust coefficient

C_P = Power coefficient

C_Q = Propeller torque coefficient

n = Rotational speed

D_p = Propeller diameter

T_r = Thrust

P = Power

D = Drag

L = Lift

ρ = Density

S_w = Wing wetted surface area

$\dot{h}$ = Rate of climb

θ = Angle of attack

Abstract

Hybrid-Electric aircraft powertrain modeling for Unmanned Aerial Systems (UAS) is a useful tool for predicting powertrain performance of the UAS aircraft. However, for small UAS, potential gains in range and endurance can depend significantly on the aircraft flight profile and powertrain control logic in addition to the subsequent impact on the performance of powertrain components. Small UAS aircraft utilize small-displacement engines with poor thermal efficiency and, therefore, could benefit from a hybridized powertrain by reducing fuel consumption. This study uses a dynamic simulation of a UAS, representative flight profiles, and powertrain control logic approaches to evaluate the performance of a series hybrid-electric powertrain. Hybrid powertrain component models were developed using lookup tables of test data and model parameterization approaches to generate a UAS dynamic system model. These models were then used to test three different hybrid powertrain control strategies for their ability to provide efficient IC engine operation during the charging process.

The baseline controller analyzed in this work does not focus on optimizing fuel efficiency. In contrast, the other two controllers utilize engine fuel consumption data to develop a scheme to reduce fuel consumption during the battery charging operation. The performance of the powertrain controllers is evaluated for a UAS operating on three different representative mission profiles relevant to cruising, maneuvering, and surveillance missions. Fuel consumption and battery state of charge form two metrics that are used to evaluate the performance of each controller. The first fuel efficiency-focused controller is the ideal operating line (IOL) strategy. The IOL strategy uses performance maps obtained by engine characterization on a specialized dynamometer. The simulations showed the IOL strategy produced average fuel economy improvements ranging from 12%-15% for a 30-minute mission profile compared to the baseline controller. The last controller

utilizes fuzzy logic to manage the charging operations while maintaining efficient fuel operation where it produced similar fuel saving to the IOL method but were generally higher by 2-3%. The importance of developing detailed dynamic system models to capture the power variations during flight with fuel-efficient powertrain controllers is key to maximizing small UAS hybrid powertrain performance in varying operating conditions.

Chapter 1. Introduction

1.1. Motivation and Problem Statement

The desire to reduce vehicle greenhouse gas emissions from fossil fuel-based propulsion systems has created a growing interest in hybrid propulsion system. This reduction in fossil fuel usage is mainly accomplished by introducing more electrified forms of propulsion into vehicles, such as hybridized vehicles. In the automotive industry, various implementations of hybrid powertrains combining internal combustion (IC) engine with an electric motor have been used to reduce vehicle fuel consumption and emissions considerably. A hybrid vehicle is generally defined as any vehicle that implements two distinct forms of power for propelling the vehicle. Different forms of hybrid systems such as gasoline-hybrid powertrain vehicles or fuel cell-electric hybrid systems have been developed and shown to be feasible. The interest in hybrid aircraft was sparked when automobiles began to implement hybrid powertrain technology and successfully reduce emissions. Numerous techniques have been utilized to reduce emissions, such as using smaller displacement 4-cylinder engines, which use less fuel than typical engines that propel vehicles now. Another method used is regenerative braking, where energy from decelerating the vehicle is harvested and converted to electrical power. This method essentially reuses energy that would be otherwise wasted, which can now, in the form of electrical power, be used to propel the vehicle [1]. Likewise, next-generation aircraft seek to leverage hybrid electric powertrain technology to reduce fuel consumption and emissions by using more electrified forms of propulsion, which also have the added benefit of reduced noise. This increasing interest in hybrid technology has obviously created new engineering challenges for the aviation industry. Challenges such as designing a hybrid propulsion system without affecting the aircraft's current performance in terms

of payload weight capacity, range, and endurance is of great importance, but being able to surpass that performance mark is the ultimate goal.

Research and development into all-electric and hybrid-electric aircraft propulsion are ongoing at leading aviation companies and national laboratories [2]. Airbus and Rolls Royce are currently collaborating on a series hybrid aircraft concept called the E-Fan X. This aircraft uses the BAe 146 regional plane as a testbed with one of the aircraft's four gas turbine engines replaced by a 2 MW electric motor [3]. Other hybrid electric aircrafts concepts exist, as shown in Figure 1, such as the CENTERLINE concept, which uses a propulsive fuselage concept that places a turbo-electric propulsor in the tail of the aircraft. Another hybrid aircraft in development by Boeing called SUGAR Freeze, utilizes a liquefied natural gas fuel cells to electric power motors. Lastly, an all-electric aircraft being developed by NASA called the X-57 Maxwell utilizes 14 electric motors to provide sufficient thrust. Its ultimate design goal is to achieve a 500 percent increase in high-speed cruise efficiency [4].

(a) Bauhaus Luftfahrt CENTERLINE [5]

(b) Boeing SUGAR Freeze [6]

(fig. cont'd.)

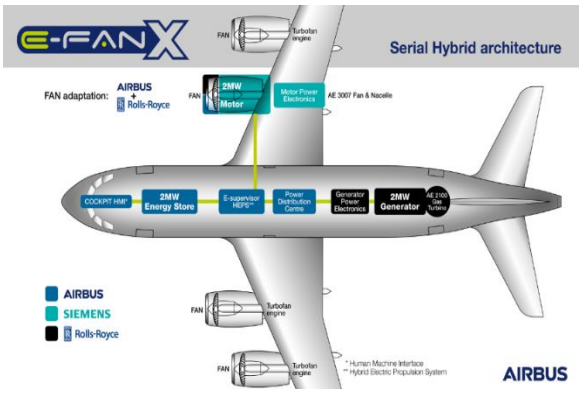

(c) Airbus E-Fan X [3]

Figure 1. Hybrid aircraft concepts

Some functioning prototypes for hybrid aircraft have been developed and tested. One example of a functioning hybrid aircraft is shown in Figure 2 of the Siemen's DA36 E-Star 2 aircraft, which utilizes a hybrid powertrain implemented in a series configuration. The Siemen's aircraft successfully completed a one-hour flight at the Paris Air Show in 2013 and claimed a 25% reduction in fuel consumption and emissions [7]. The HY4 is another hybrid aircraft that first took flight in 2016 and has a fuel cell hybrid powertrain. The HY4 claims to be able to achieve a range of between 750-1500 km depending on flight conditions [8]. As one can see, many different forms of hybrid powertrains are being explored and, more specifically, hybrid electric powertrains. A hybrid vehicle is generally defined as any vehicle that implements two distinct forms of power for propelling the vehicle. Different forms of hybrid systems such as fuel cell hybrid systems have been developed and shown to be feasible. However, hybrid powertrains mainly considered practical for use in transportation consist of petroleum-electric hybrid considering current technology with fuel cell-electric hybrids becoming increasingly popular and may become feasible powertrains in the near future. The hybrid-electric powertrain class that is the main focus of this work because this hybrid technology is proven and mature. Thus, the only development needs for

use in aircraft is integration into a functional aircraft propulsion unit and development of control systems to ensure the system performs at optimal conditions.

(a) Siemens series hybrid drive system [7]

(b) HY4 [9]

Figure 2. Existing hybrid aircrafts

Hybridization strategies discussed earlier in this section for conventionally sized aircraft are of high interest in unmanned aerial systems. Considering that hybrid powertrain technology is scalable, powertrain components like engines, motors, batteries are available across a wide range of sizes and can be scaled up or down to function in many cases. This work further focuses on the hybridization of unmanned aerial systems (UAS). UAS cover a broad range of aircraft, which has three classifications, as defined by the USAF shown in Table 1.

Table 1. UAS group specifications

	UAS Groups	Maximum Weight (lbs)	Normal Operating Altitude (ft)	Speed (kts)	Representative Aircraft
SUAS	Group 1	0-20	< 1200 AGL	<100	 *Raven RQ-11*
	Group 2	21-55	< 3500 AGL	<250	 *Scan Eagle*
	Group 3	<1320	< FL 180	<250	Currently no USAF program for this category

This work interest is mainly in small UAS (SUAS), classified as UAS operating below 3500 ft. with endurance less than 15 hours [10]. A more detailed focus is placed on Group II UAS

because this class of aircraft is generally powered by small IC engines, which makes it a good candidate for adopting a hybrid powertrain. While group 1 aircraft can be hybridized, they are typically smaller, making it challenging to implement a full hybrid system. The smaller footprint is also why group 1 aircraft are usually fully electric systems, which is more suited for the small footprint of group 1 aircraft. The aircrafts shown in Figure 3 depict two examples of group 2 UAS, which are the Boeing Insitu ScanEagle and the AAI Aerosonde. These are popular UAS platforms used by various defense services that are powered by small IC engines and could show performance benefits from powertrain hybridization, such as the benefits listed below:

- Reduced aircraft noise signature through utilizing all-electric propulsion.
- Dual power source capability providing redundancy in case of failure of either propulsion motor.
- Reduced downtime for the aircraft because battery recharging is unnecessary when a generator is on board the aircraft.
- Electric propulsion is unaffected by density altitude and allows for downsizing the ICE.

(a) Boeing Insitu ScanEagle UAV [11]

(b) AAI Aerosonde [12]

Figure 3. Group 2 UAS aircrafts

However, the challenge of hybridizing an aircraft is the weight created by the batteries in the powertrain electrification process. Aircraft design aspects such as payload weight, thrust, and

lift are all impacted by this increase in aircraft weight resulting from electrification. Therefore, when introducing a hybrid powertrain configuration into an aircraft, the components must be carefully selected for power, weight, and efficiency to have optimal performance. Also, a robust and efficient energy management control strategy is needed so that the aircraft can perform the same or better than a conventional aircraft. The efforts in this paper focus on exploring the effects of hybridizing a group 2 UAS, where the primary goal is reducing fuel consumption, which is a particular concern for UAS in group 2 because of the small, inefficient 2-stroke engines use in this platform.

1.2. Research Objectives

1. Analyze series hybrid powertrain performance for representative UAS taking into account detailed performance characteristics of individual components as well as dynamic effects imposed by the aircraft mission profile.
2. Develop and evaluate control schemes for series hybrid powertrains and compare their relative benefits or deficiencies.

1.3. Approach

- Develop a dynamic powertrain model simulation for a series hybrid powertrain for a representative group 2 UAS aircraft.
- Incorporate detailed performance maps for individual powertrain components either from models with tuned parameters or measured performance data through lookup tables.
- Develop different control approaches that aim to reduce fuel consumption and compare to a baseline control scheme.
- Develop a hardware in the loop (HIL) testbed to validate the powertrain model, test the various control schemes, and optimize or tune the model for accuracy.

1.4. Thesis Structure

This thesis is organized into seven chapters that detail the theory, modeling, and analysis of a series hybrid electric powertrain for a UAS. Chapter 2 provides a literature review of hybrid powertrains concepts where a review of the various powertrain configurations are explored in addition to the number of design challenges of hybridizing a UAS. A review of the advantages and disadvantages of conventional petroleum-powered aircraft and electric-powered aircraft is offered, where an explanation of the benefits of combining these two forms of propulsion into a hybrid system is discussed.

Chapter 3 provides a detailed explanation of the integrated HEUAS series powertrain model. The various component models composing the hybrid system are discussed in terms of their development, performance, and role in the system model. Also, a set of mission profiles are presented and discussed, which serve as the test cases for the powertrain to simulate different flight situations or missions that a UAS will typically perform.

Chapter 4 discusses the three different control approaches used in this analysis to determine the fuel-efficient operation of the hybrid powertrain. This section will mainly focus on the Ideal Operating Line (IOL) controller development and the fuzzy logic controller and its focus on fuel efficiency.

Chapter 5 discusses the results of the three individual control strategies and their effect on the performance of the hybrid powertrain for the three different mission profiles addressed in chapter 3. A comparison of the three different control strategies is also discussed where the control strategies are analyzed for their effectiveness to reduce fuel consumption over the 30 min mission duration for the three different mission profiles.

Chapter 6 describes the hardware test stand developed for a series hybrid powertrain and describes what instrumentation and components were used in its development. In this section, a detailed explanation is given for how these various components interact and what information and data are collected to aid in validating the powertrain model simulation.

The last chapter contains the concluding remarks, recommendations, and the next steps for hybrid powertrain modeling, control, and testing.

Chapter 2. Literature Review and Theory

2.1. Introduction to UAS Hybrid Powertrains

2.1.1. Series Hybrid Configuration

Many hybrid propulsion systems are petroleum-electric based because of its simplicity and ease of integration. Within this class of hybrid electric powertrains, three different powertrain configurations are possible, which are series, parallel, and split power. Each of these configurations have their pros and cons, such as increased packaging weight or reduced versatility.

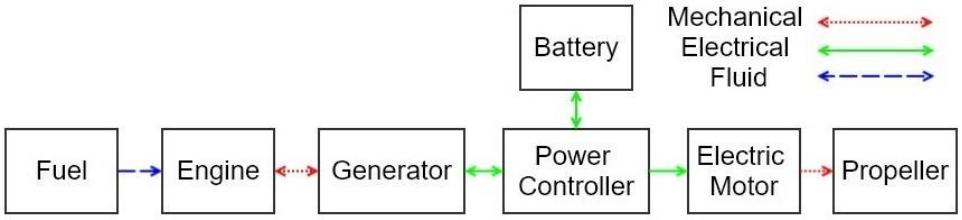

Figure 4. Series hybrid configuration

The series configuration (Figure 4) is the simplest powertrain type consisting of electric motors (EM), batteries, and internal combustion (IC) engine with a generator. The series hybrid vehicle's propulsion is purely derived from electric motors. An IC engine serves as an auxiliary source of power for the electric motor when the batteries require charging. The IC engine during charging periods operates at some optimum point to reduce fuel consumption. The series HEV is advantageous in many aspects in comparison to other HEV architectures listed previously. For example, no mechanical path exists between the engine and the propeller, enabling the ICE to operate in a peak-efficiency zone and reduce fuel consumption. The absence of a mechanical connection also reduces the space need for the powertrain. Also, when compared to parallel and power-split configuration hybrid vehicles, the series HEV can be adequately managed using a relatively simple control scheme [13]. However, some disadvantages exist for the series hybrid powertrain as outlined in [13], which are:

- Multiple energy conversions are needed, which reduce the overall efficiency of series HEV, especially when the vehicle is at high speed
- The propulsion motor is the only direct power source, which means the motor and its supporting electronics should meet maximum power demand, thus requiring more robust construction which increases cost, weight, and volume requirements
- The power of the engine is unable to be provided directly to the propeller if the propulsion motor fails.

2.1.2. Parallel Hybrid Configuration

The parallel (Figure 5) configuration, similar to the series configuration, contains EM, batteries, and an IC engine. However, the parallel hybrid powertrain is a more complex powertrain type where EM and the IC engine are coupled to both power the vehicle. Parallel hybrid powertrains connect the engine and electric motor to operate at a fixed speed ratio to provide driving torque to the wheel, separately or together [13].

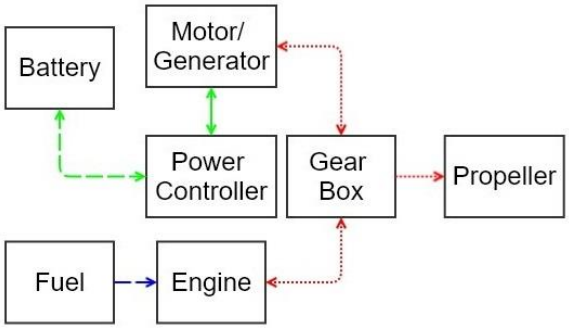

Figure 5. Parallel hybrid configuration

Parallel configurations usually contain a gearbox to couple the power from both the EM and IC engine to distribute power to the propeller, which means that both motors must run at the same speed in dual power mode. This also means that the addition of a gearbox can potentially increase system weight and limit payload capacity. However, the addition of a gearbox allows for

better control of power flow as needed. This means that the EM can also work as an engine booster or generator to optimize the efficiency of ICE, according to battery SOC and system load [13].

Moreover, the parallel system can generate power to charge the batteries like the series configuration but because there is no second EM for dedicated power generation. The same EM used for propulsion must also function as a generator during battery charging operations. This implies that the EM is not able to provide propulsive power during the charging process, and propulsion is purely supplied by the IC engine. Thus, if the aircraft undergoes a scenario where the engine is not able to provide the necessary torque or power to meet the demand while the battery SOC is low and charging is a high priority, the EM will not be able to assist the IC engine in meeting the power demand. Most parallel hybrid systems seen in automobiles utilize other methods to recharge the batteries, such as regenerative braking [14]. Unfortunately, in an aircraft, this is not a concept that is always feasible. Some researchers have explored different techniques to harvest energy, such as in [15], where thin-film photovoltaics are explored for range-extending capabilities or a windmilling design explored in [16].

2.1.3. Series-Parallel Hybrid Configuration

Lastly, the power-split (Figure 6) or series-parallel configuration combines both aspects of the series and parallel systems. Power-split powertrains are similar to the series configuration and have a dedicated generator for supplemental power for charging batteries. Also, the energy from the IC engine and EM can be coupled together via a gearbox to provide propulsion for the vehicle similar to the parallel system. This gearbox is often called a power split device, which is usually a single planetary gear set or a compound planetary gear set. This gear set is responsible for splitting the engine torque into two parts delivered to the output shaft. The planetary gear set allows for the rotational speeds of three individual gears (sun gear, ring gear, and carrier gear) to provide

independent rotation of ICE and thus enable the engine to be controlled to operate within a peak-efficiency zone. Since this configuration allows the IC engine to operate efficiently, the power-split design can achieve significant efficiency, and this configuration is very prevalent in the automotive hybrid vehicle sector [13].

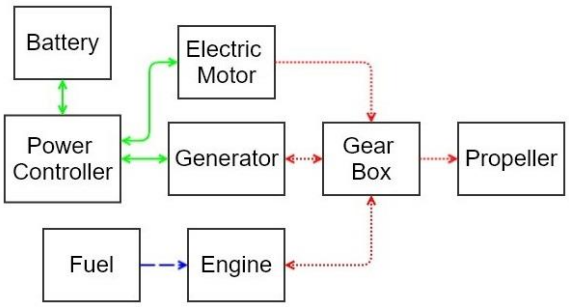

Figure 6. Power-Split hybrid configuration

An example of a successful and the most notable power split system currently in use is the Toyota Prius. The Prius is a series-parallel system that utilizes a compound planetary gear set to distribute the power from the IC engine to the generator and the wheels for propulsion. The system also couples the electric traction motor to further distribute power for accelerating the vehicle. The compound planetary gear system was implemented in later generations to extend the operating range at higher speeds. With so many different hybrid electric configurations possible, it becomes difficult to decide which system is best to use in an aircraft. Ultimately the use of a specific configuration is dependent on vehicle usage and design requirements. These various configurations allow for flexibility in designing a hybrid aircraft to fulfill numerous requirements such as increased range or redundancy. For this work, the focus was placed on the series hybrid configuration because it best fits the needs of the group 2 UAS. The series configuration was also chosen for its simplicity in developing a control strategy and the relative ease of developing a hardware test stand to test the control scheme.

2.2. Issue with Current UAS Powertrains

The benefits of hybridization are well known in terms of fuel efficiency and range-extending in ground vehicles, and adaptation into aircraft is the next logical step. Consequently, some challenges exist which are unique to aircraft, one of which is weight. Aircraft have strict weight requirements, and all the powertrain components of the aircraft must be chosen such that the performance of the aircraft is not hindered. Aircraft design aspects such as Gross Take-off Weight (GTOW), payload weight, thrust, and lift are all essential parameters that are linked together and affect performance.

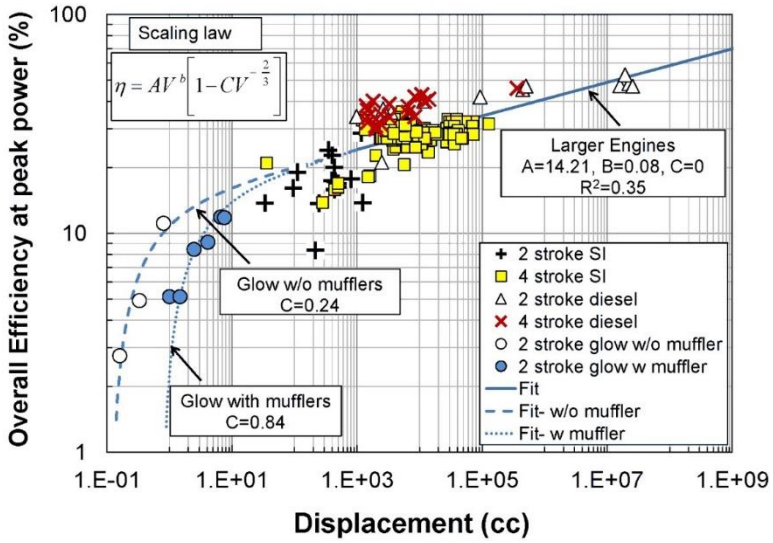

Figure 7. Scaling of overall efficiency with engine size [17]

Therefore, when introducing a hybrid powertrain configuration into an aircraft, the components must be carefully selected for power, weight, and efficient performance so that the aircraft can perform the same or better than a conventional aircraft. This aspect of component weight is underscored when you consider the batteries required in a hybrid powertrain. The primary source of weight in hybrid vehicles is the battery due to their low specific energy, which ranges from ~100-200 Wh/kg (0.9 MJ/kg) [18]. When compared to gasoline, which has a specific energy of ~45 MJ/kg, this energy density difference is nearly 50x greater for gasoline, and it is

apparent that more battery mass is needed to match the energy capacity of most petroleum-based fuels, and this is the case for even the most advanced lithium-ion batteries.

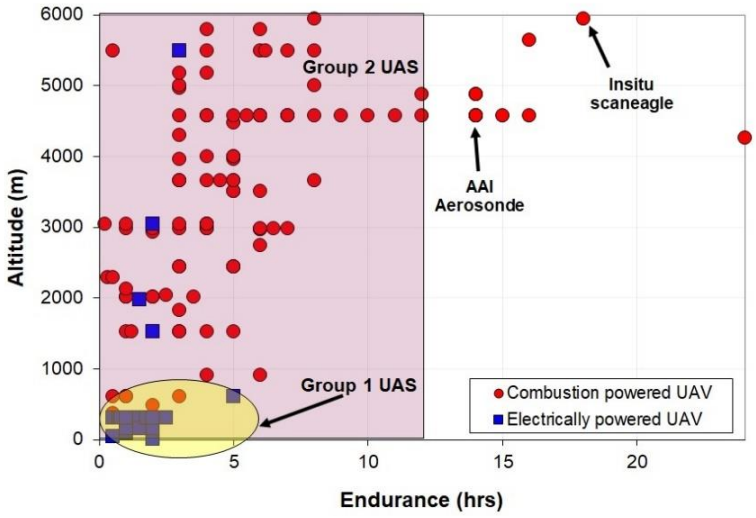

Figure 8. UAS endurance [17]

Fortunately, higher energy density batteries (500-1500 Wh/kg) are under development, and [19] offers a review of various battery chemistries under development that hope to narrow the performance gap between petroleum fuels. Cell chemistries such as lithium-sulfur or lithium-air batteries have hopes of achieving energy densities of ~350-390 Wh/kg [20,21] and 1700 Wh/kg, respectively [22]. However, because of the increased weight of batteries alone in hybrid powertrains apart from the other added components in the system, an impact on the aircraft range and endurance is expected.

Figure 9. Pipistrel ALPHA ELECTRO [23]

Figure 10. NASA X-57 [4]

Aircraft performance, particularly concerning range, can be studied by considering the Breguet range equation for fuel- and electric-powered aircraft operating at cruise, as shown in Eq. (2.1) and (2.2). For an aircraft with a given lift-to-drag (L/D) ratio, the range is directly related to three terms – energy density of the power source (QR or QB), its efficiency (ηoverall), and the weight fraction (mfuel/mtakeoff or mbattery/mtakeoff). Observation of Eq. (2.1) and (2.2) demonstrate petroleum-based aircraft have a better range because, during flight, fuel is consumed, which reduces power requirements during flight, thus increasing range. In contrast, battery-powered aircraft do not have this benefit. However, as shown in Figure 7, Eq. (2.1) is highly affected by efficiency, caused by the engine size and surface to volume ratio. For these small displacement, 2- stroke engines, a rapid dropoff in efficiency are observed at the smallest scales resulting in reduced range. UAS range and endurance metrics observed in Figure 8 show that most aircraft with a maximum altitude below 500 ft. are powered electrically and have low endurance. This observation is mainly the result of the group 1 aircraft size restrictions, which are better suited to electrification. While the rest of the aircraft listed in Figure 8 are powered using hydrocarbon-fueled combustion reciprocating IC engines and have considerably higher endurance metrics.

The main advantage of using combustion-based devices is the high energy density of the fuel, enabling higher range and endurance of the aircraft. Therefore, one can conclude that

electrified forms of aircraft prolusion have low endurance due to the low specific energy of the battery power source. Fully electric aircraft currently in existence, such as those shown in Figure 9 and Figure 10, typically have range and endurance metrics much lower than their petroleum-based counterparts. The Pipistrel fully electric aircraft shown in Figure 9 advertises a range of 75 NM (86 mi) and endurance or 60 min. In comparison, the petroleum-based version of the same aircraft can achieve 324 NM (372 mi) of range and endurance of 3.6 hr. This implies that hybridizing an aircraft can adversely affect the endurance or range if the battery capacity isn't able to meet the requirements of the aircraft. This adverse effect on range and endurance is mainly due to the low energy density of batteries.

$$Range = \frac{Q_R}{g}\eta_{overall}\frac{L}{D}\ln\left(\frac{1}{1-\frac{m_{fuel}}{m_{takeoff}}}\right) \tag{2.1}$$

$$Range = \frac{Q_B}{g}\eta_{overall}\frac{L}{D}\frac{m_{battery}}{m_{takeoff}} \tag{2.2}$$

Research performed by Schömann [24] on hybrid powertrain development focused on the accuracy, high computational efficiency, and generic applicability of modeling a hybrid powertrain's performance. Schömann analyzed the effect that the electric flight time had on the hybrid aircraft weight and fuel consumption. He found that as one increases the potential electric flight time or ratio of electric flight time to the total flight time of the hybrid system, the takeoff mass of the aircraft increases. This is because of the increased battery mass required to achieve higher flight times, making the aircraft infeasible [24]. Schömann determined that for an aircraft with a required flight time of 5h 30min or less, a flight time ratio of 0.25 provides optimal fuel efficiency. For flight time ratios from 0.50-0.75, the only benefit of hybridization is to have one of the propulsion units act as a power booster for climbing segments or high-power demand periods. Therefore, Schömann essentially determined that the amount of electric-only flight time,

which is directly related to the battery capacity or battery mass, can have an adverse effect on the efficiency of the hybrid powertrain. Meaning that once you add a certain amount of battery mass such that you design your aircraft to be capable of providing more than 25% of electric-only flight time, the fuel efficiency gains offered from the hybrid powertrain begin to diminish. These findings are logical because it outlines the dilemma of hybridizing an aircraft, determining a balanced ratio between the battery mass and fuel mass which provide the best efficiency and performance.

Moreover, group 2 UAS utilizes small-displacement engines with low thermal efficiencies of 4-18% and high fuel consumption [25]. Due to this low efficiency, this class of aircraft could benefit from a hybrid powertrain where propulsive power can be supplemented by electrical energy. This also shows the importance of battery capacity sizing in terms of system efficiency. The low efficiency of the IC engines used in this class of aircraft dictates that ample fuel is onboard the hybrid aircraft. The engine is effective and does not run out of fuel quickly during a mission. Therefore, the hybrid aircraft must be designed to have the proper battery capacity and fuel to complete desired missions and be as efficient as possible.

2.3. Challenges and Advantages for Hybridizing Aircraft

Range equations for series and parallel hybrid powertrains presented in Eq. (2.3) and (2.4), respectively, were adapted from [26]. Slight modifications were made to Eq. (2.3) and (2.4) to include additional efficiency terms for the IC engine and the electric motor to reflect the total efficiency of the hybrid powertrain. Also, the lift-drag ratio term was changed to reflect in terms of the total lift and drag rather than the lift-drag coefficients. These range equations presented some challenges because they are not as straightforward to analyze since new terms such as the degree of hybridization (Ψ) and power split (S) are introduced. The former refers to the relative amount of energy stored in the battery vs. the fuel onboard the hybrid aircraft.

In contrast, the latter refers to power supplied by the electrical unit compared to that by the IC engine. Considerations for the degree of hybridization and power split are strongly linked to the UAS mission profile and powertrain control logic, which are not captured by range equations in Eq. (2.3) and (2.4). The performance of hybrid-electric powertrains for small UAS is difficult to predict using range equations for cruise or the optimal design and sizing approaches developed in previous work. These approaches do not fully consider the close coupling of the aircraft mission profile with the performance of individual hybrid powertrain components, which can vary significantly throughout the mission. Further, previous efforts have relied on manufacturer supplied data for IC engine performance, which can be limited to a single operating point and often overstated for small IC engines used in UAS applications [27,28]. Moreover, powertrain performance is strongly linked to the control logic used to operate the hybrid-powertrain, which needs to be incorporated into the analysis

$$Range = \eta_{elec}\eta_{eng}\eta_{prop}\frac{L}{D}\frac{1}{g}\left(\frac{Q_B Q_R}{\psi Q_R + (1-\psi)Q_B}\right)\ln\left[\frac{W_e + W_{pl} + \left(\frac{(\psi Q_R + (1-\psi)Q_B)}{Q_B Q_R}\right) g E_{start}}{W_e + W_{pl}}\right] \tag{2.3}$$

$$Range = \frac{1}{\left(\frac{1-S}{\eta_{ov,mech}} + \frac{S}{\eta_{ov,elec}}\right)}\frac{L}{D}\frac{1}{g}\left(\frac{Q_B Q_R}{\psi Q_R + (1-\psi)Q_B}\right) ln\left[\frac{W_e + W_{pl} + \left(\frac{(\psi Q_R + (1-\psi)Q_B)}{Q_B Q_R}\right) g E_{start}}{W_e + W_{pl}}\right] \tag{2.4}$$

While several entities are trying to develop UAS with hybrid powertrains, there is a lack of publicly available data concerning their performance or capabilities. Limited availability of data can be attributed to technological challenges in developing hybrid powertrains and a lack of public release of open data by groups developing such systems. In the absence of published performance data for small UAS, some insights can be obtained from previous studies on the sizing of hybrid-electric powertrains for small UAS. The concerns mentioned above about the increased weight of aircraft with hybrid powertrains have motivated several groups to conduct studies on size and weight optimization [26]. These studies have focused on estimating the weight fractions of

different hybrid powertrain configurations for use in a given unmanned aircraft with a fixed mission profile [29]. The previous studies generally pursued an iterative design approach that predicted sizes for the engine or the motor without particular regard to practically available components [30]. Further, the component performance was generally obtained from manufacturer specifications or scaling arguments.

Sizing is strongly affected by the powertrain mechanical configuration, such as series, parallel, or power-split. A sizing analysis done in [31] utilized the Breguet range equation for fully electric and petroleum-based powertrains (Eq. (2.1),(2.2)) described in the previous section to provide range and endurance estimates for a retrofitted hybrid system. In their work, they concluded that to have an equal hybrid electric range and endurance performance compared to fuel-powered powertrains, the battery specific energy of current Li-Po would have to be increased by 2.4 times the current energy density. Work conducted by Donateo et al. [32] focused on sizing components such as the battery and electric motor for evaluating the endurance of a parallel hybrid-electric aircraft. In their work, they discuss the effect of battery sizing and engine operating points on fuel economy. They found that when batteries are appropriately sized for a 30 min flight time, a 12% reduction in fuel consumption can be observed over a non-hybrid system. Another sizing study performed by Hiserote in [33] conducted a conceptual design of three variations of a parallel hybrid-electric propulsion system for a small UAS. In this study, the hybrid-electric system designs were optimized and compared to determine the most suitable design for a typical UAS mission. The work conducted by Hisrote was later continued by Rotmal in [34], where further optimization for the sizing and optimization of the propeller and motor combination was done. Lastly, others have employed more sophisticated forms of sizing techniques for hybrid powertrain components using genetic algorithms in [35] or using a multidisciplinary coupled derivative approach in [36],

where more aspects and factors of hybrid powertrain performance and operation are integrated into the sizing analysis.

The key aspect of these design and sizing studies was to find optimally sized components for the hybrid-electric powertrain to achieve range/endurance improvements, primarily at cruise conditions. However, little to no consideration was given to the significant variation in the performance of individual components and the integrated hybrid powertrain resulting from changing flight conditions, commonly observed in UAS operation. However, the benefits for UAVs could offer a substantial number of benefits, especially for drones explicitly designated for surveillance and reconnaissance. Benefits such as increased range, endurance, and reduced sound signature can allow for more extended surveillance missions with lesser chances of detection. The possibility of having a minimal sound signature is further realized when propeller design optimization is coupled with hybrid powertrain development. Work conducted by [37] focused on optimizing propeller geometry to reduce the noise production of propellers for small UAVs. The increased range and endurance aspect for UAVs allows for possibilities to have long continuous periods of flight. This gives a tactical advantage to operators because of the ability to gain more information during a mission. For commercial aircraft, a hybrid powertrain could mean a significant reduction in carbon emission and a reduction in fuel costs. With aircraft accounting for 9% of the total greenhouse gas emission in the transportation sector, according to the EPA, hybrid propulsion could provide a significant emission reduction. Battery technology advancements are trending in a direction to achieve higher energy density, thus narrowing the gap between fuels making hybrid systems more viable. If one also considers future advancements of more efficient forms of energy harvesting such as solar cells, then fossil fuel emission could reach a near net-zero level where regional and international travel are all feasible without using fossil fuels. However,

until these advancements in battery and solar cell technology come into existence, work needs to be done to make our current technology and systems more efficient. This leads to the next task, which is being able to operate aircrafts engines in a very efficient manner or region of operation. These efforts will increases system efficiency overall; however, this requires significant effort in powertrain control systems development so that each component of the powertrain can operate efficiently and achieve the best performance.

2.4. Hybrid Powertrain Control Methods

The main functions of a powertrain control system is to regulate power flow for optimal performance of each component and the overall system. It also must ensure seamless operation and communication of all powertrain components to allow for safe operation within defined limits. When implementing a hybrid system for this class of UAS or any sized aircraft, careful consideration of the control strategy is necessary. Powertrain performance is strongly linked to the control logic used to operate the hybrid-powertrain, aiming to increase the overall powertrain efficiency by minimizing fuel consumption or optimizing power usage.

Many control methods have been implemented on hybrid power-trains, as depicted in Figure 11, all ranging in complexity and form. A review conducted in [38] provides an overview of various control methods implemented in the automotive industry for hybrid power-trains. Some control strategies that have been implemented are more deterministic such as in [39]. In these more deterministic control schemes, functional mapping is used to operate the hybrid powertrain in a charge sustaining or charge depleting mode where the SOC is maintained at a set level.

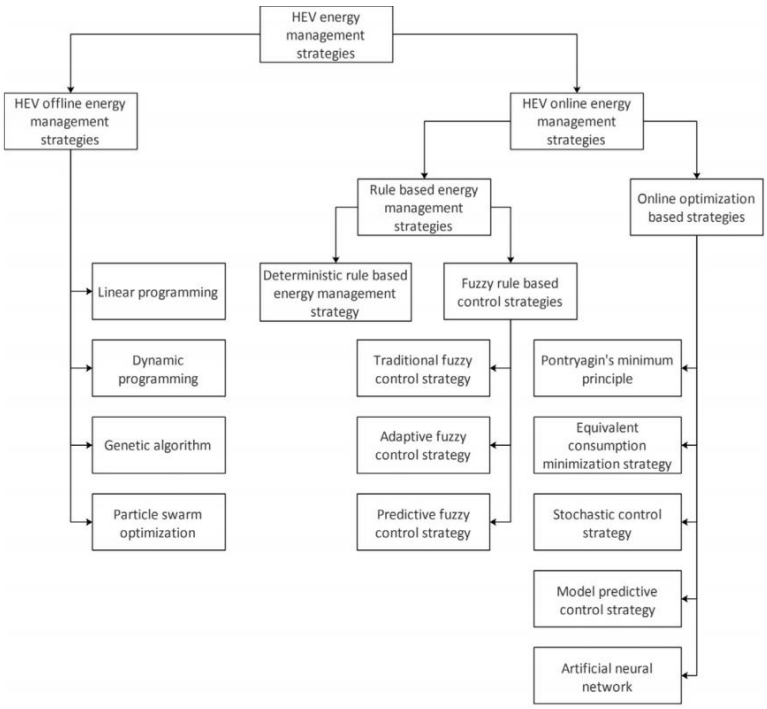

Figure 11. HEV powertrain control space diagram [38]

These deterministic forms of control are very easily implemented and prioritize electric-only operation, which doesn't always manage to reduce fuel consumption; however, they do not consider the efficiency of the engine when in operation or have an emphasis on energy optimization. Other control strategies have focused on energy management or optimization strategies to maximize efficiency. In a study by Gao et al. [40], three different control strategies were analyzed: thermostat control, power follower control, and an equivalent fuel consumption optimal control strategy. These control strategies were investigated for increased fuel economy of a series hybrid powertrain where they determined that an equivalent fuel consumption optimal control method offered the most fuel savings due to the ability of the controller to optimize the power distribution between the engine-generator and battery. Another researcher explored the performance differences between a passive and active power management scheme for a solar/fuel cell hybrid powertrain. Their results showed that for a 4.5 hrs simulation, the passive management

strategy operated reasonably well with the solar/fuel cell providing the majority of power with the battery only functioning as supplemental power during peak power demands. However, the passive nature of the schemes was not able to reserve power from either power source when solar power was low or distribute power during times of peak power demand [41]. They also showed that the active management strategy, which uses a thermostat control approach to distribute power, was able to maintain a minimum level of SOC for the battery, resulting in efficient power distribution and greater system safety.

Furthermore, numerous studies have been performed, which focus more on engine fuel efficiency. One control strategy developed in [42] used an algorithm to minimize fuel consumption for a series hybrid powertrain. Further research performed by [43–45] employed an Ideal operating Line (IOL) control approach for a parallel hybrid powertrain configuration. In the IOL scheme, an engine efficiency map is used to define a line of best efficiency, which traces the operation path that the engine should follow. The goal of this method is to provide a simple deterministic approach to operate the engine in an efficient manner that does not rely on non-linear forms of control. The control methods presented thus far are all considered deterministic and rely on some prior knowledge of the system, and generally will produce the same output for a given input. In contrast, non-deterministic forms of control function more in terms of probabilistic outputs where given the same input, at different points in time, a different output can be produced.

Other non-deterministic forms of control have also been analyzed, which are more predictive in function and may utilize future information to influence the current output. These forms of control typically are better suited to optimize the powertrain operation for the best fuel economy. The optimal strategy present in [46] is an online optimization strategy where better results were observed over the deterministic forms of control. A cerebellar model arithmetic

computer (CMAC) control approach was developed for a parallel hybrid in [47] based on a neural network. This controller focused on optimizing the engine torque control surface to develop more efficient battery charge-sustaining or charge- depletion control. This CMAC control was able to reduce energy usage by 6.5% in comparison to a rule-based controller they also developed. Another popular control commonly used in hybrid vehicle control is a model predictive controller (MPC). An MPC controller presented in [48] developed a model predictive control with a torque-split strategy to reduce fuel consumption for a parallel powertrain configuration. This MPC strategy was designed to provide better operation during a transient process where it was able to reduce fuel consumption by approximately 500 g in comparison to a typical PID-based SOC regulation strategy.

However, developing online optimization control strategies may not be necessary if the transient operation or the need to find optimality isn't a priority or the predictive ability of MPC's and neural networks are not needed. If accurate test data or information is available for modeling system components such as the engine, then using a deterministic control strategy can be equally capable of providing efficient engine operation. However, deterministic control methods do have limitations in the degree of freedom of control, limiting the number of variables that can be optimized [38]. Fuzzy logic controllers are one deterministic controller that allows for more degrees of freedom and can allow for a number of variables to affect the control output. A fuzzy logic control approach proposed in [49] analyzed the ability to reduce fuel consumption for a series hybrid vehicle where it could effectively regulate the power flow of the powertrain while maintaining the SOC of the batteries at a high level. Another series hybrid controller based on a fuzzy logic fixed boundary-layer sliding mode controllers was able to gain a 3.73% increase in fuel economy over the conventional power follower or thermostat forms of control [50].

Chapter 3. Integrated HEUAS Series Powertrain Model

3.1. System Model Description

The model represented in Figure 12 depicts the full system model of the HEUAS, including the powertrain model, flight dynamics model, powertrain controller, and flight/mission profile used in the simulation. The model uses a forward-facing approach where information on the flight profile is passed to the powertrain controller, which produces commands to send to the powertrain model [51]. The mission profile is in the form of the desired flight speed and altitude profile used to simulate an operating scenario such as climbing, cruising, or loitering flight. This flight profile is used as an input for the powertrain controller, which produces commands to send to the powertrain model.

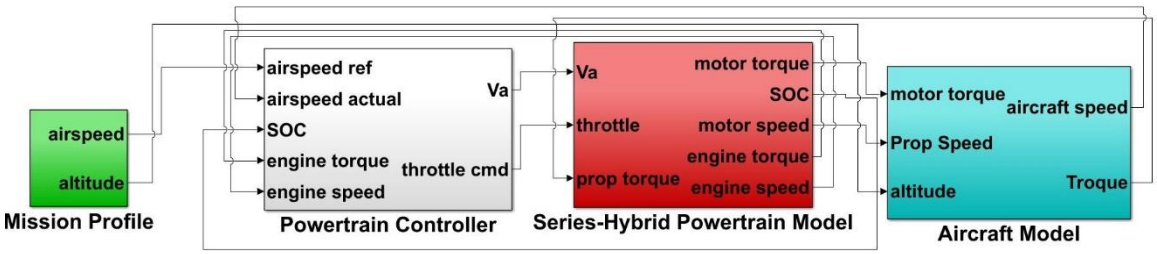

Figure 12. System model for series hybrid-electric UAS

The series powertrain model then uses those input commands for requested speed, torque, or throttle and outputs values for the torque or speed response depending on the component model. Those powertrain outputs are then passed to the aircraft model, which output the vehicle speed, which is used as one of the feedback signals for the powertrain controller. The controller output commands are then sent to the powertrain to ensure that the aircraft can maintain the flight profile while maintaining the desired state of charge (SOC) in the batteries. The dynamic powertrain model was developed using individual powertrain components, which were combined to create an integrated model. The development of component models consists of incorporating performance

maps of different hardware components and model parameter estimation using component test data. The model data and parameters were all vital for simulating the performance of the physical components of the powertrain and allows for accurate modeling of system performance. Figure 13 depicts the block diagram of the series hybrid powertrain mode and the signal flow of information. The model consists of multiple blocks where each block represents the individual component models. These blocks are created in MATLAB/Simulink and contain constitutive equations or lookup tables (LUT) of performance data, which characterizes the operation for each of the respective components in the powertrain. In the next sections, the component models used in the development of the hybrid powertrain model are described in more detail.

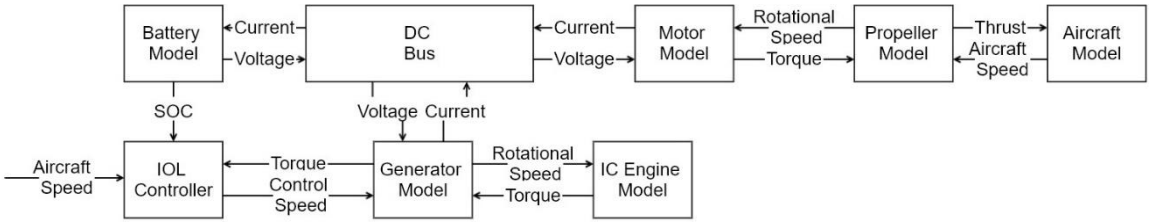

Figure 13. Series hybrid layout and signal flow

3.1.1. Electric Motor Model

Many different forms of motors exist, as shown in Figure 14, and each have unique methods of operation. Since most motors used in actual UAS are aircraft grade brushless direct current (BLDC) motors, it is only appropriate that one develops a model that accurately characterizes the motor operation based on the needs of the powertrain system model. DC motors models used in dynamic simulations have various forms and different classifications, which are used to model other aspects of the motor operation as described in [52].

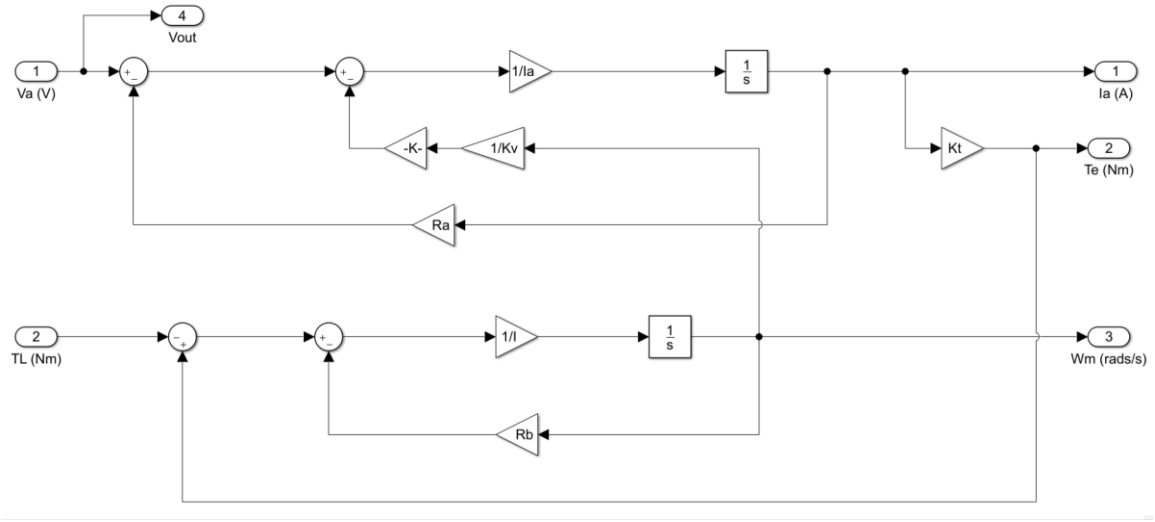

Figure 14. Electric motor Simulink model

The model one chooses to use depends on which elements of the motor's operation are desired in the system model. For example, if the powertrain system model requires that one analyze the power quality of each phase of a 3-phase motor, then one must use a model that can accurately characterize the phase voltage and current of the motor. Therefore, if one desires to model the BLDC motor to a high degree of accuracy, then it is necessary to use a mathematical model of a synchronous machine that models the function of a permanent magnet BLDC motors. However, this level of model is complex and not always necessary, especially if only a high-level system model is being developed, such as the one used in this work. Simpler models such as the series dc machine are much less complex and capture the necessary dynamics of motor operation if the model is appropriately parametrized.

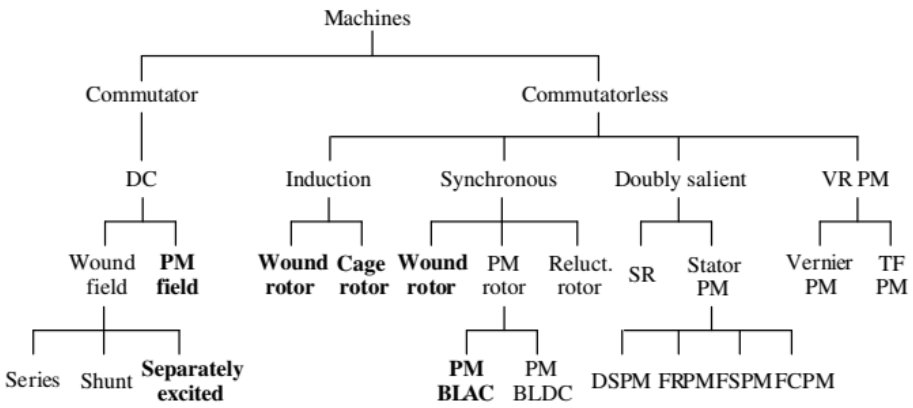

Figure 15. Electrical machine classification [52]

The motor model utilized in this work is a lumped parameter approach characterized by an equivalent circuit model for a permanent magnet DC motor, as shown in Figure 16. The mathematical equations used to model the motor are shown by Eq. (3.1)-(3.4) where the armature inductance (L), armature resistance (R), motor inertia (J), and viscous damping friction (b) are all parameters of the motor that characterize its performance including the back EMF constant K_b and the torque-constant K_t. Proper parametrization of the motor is crucial for proper validation of the motor model. Thus, parameter identification was performed where the various properties are determined using data gathered from physical motor test data for the KDE 7215XF-135 brushless DC motor.

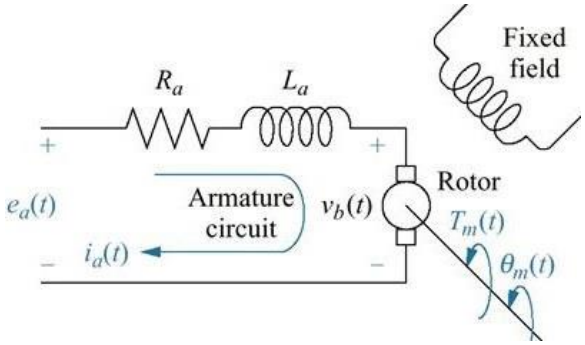

Figure 16. DC motor equivalent circuit model [53]

$$J\ddot{\theta} + b\dot{\theta} = K_t i \tag{3.1}$$

$$L\frac{di}{dt} + Ri = V - K_b\dot{\theta} \tag{3.2}$$

$$T = K_t i \tag{3.3}$$

$$e = K_b\dot{\theta} \tag{3.4}$$

Thus, data was collected for the KDE motor on speed, current, and voltage data for a ramped test up to 2100 RPM using an RC Benchmark Series 1580 Thrust Stand and Dynamometer, which will be discussed in detail later in chapter 6. This data was then used to estimate the model parameters with Simulink Design Optimization, where the test data was used to tune the model parameter until the model output matched the test data. Tuning results are shown in Figure 17, displaying good agreement between model response and measured motor speed and current draw.

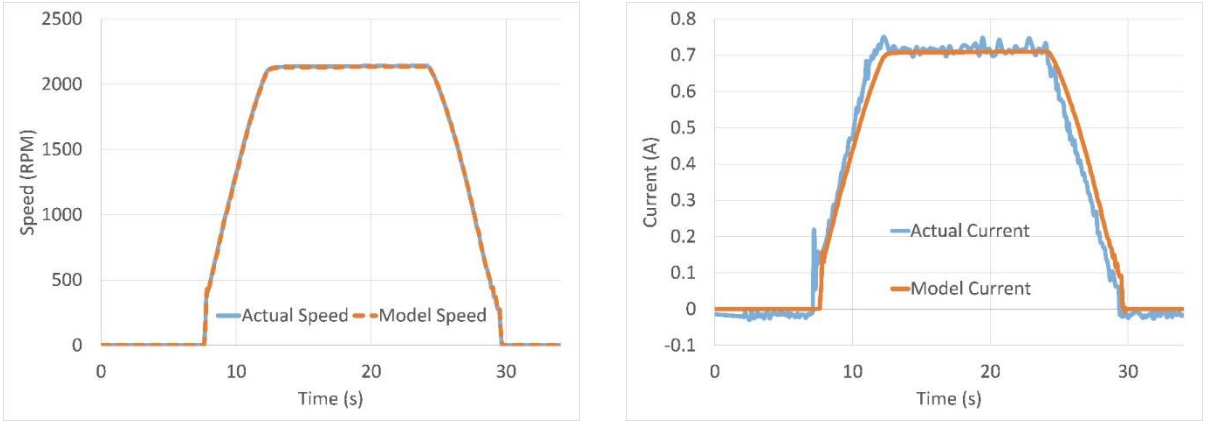

(a) (b)

Figure 17. Motor model response validation

Lastly, the motor model uses a PWM speed controller model, which was created to control the motors speed. The motor speed controller uses a cascade form of control composed of a motor speed control outer loop and a motor current control inner loop adapted from [54]. The outer speed control loop utilizes the speed command produced by the UAS pilot model, which produces an acceleration command based upon the minimum and maximum motor speed. This motor speed controller then attempts to reduce the error between the reference motor speed and the actual motor

speed feedback from the motor model. The motor speed control loop then creates a current reference used by the inner current control loop, which controls the motor current production to the reference value. The motor current controller also creates a reference voltage for use in the PWM model signal model. The PWM model utilizes the voltage supplied by the battery model and the reference voltage provided by the inner loop of the motor speed controller to give the proper PWM pulse to supply the motor model with the appropriate voltage to produce the desired motor speed.

3.1.2. Generator Model

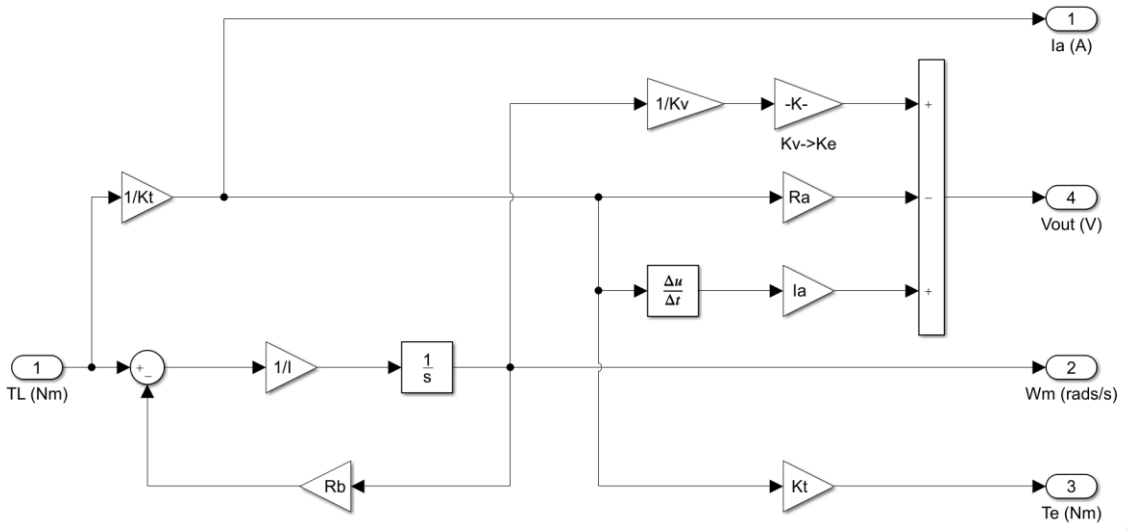

Figure 18. Generator Simulink model

The generator model (Figure 18) is fundamentally the same as the motor model, except the function is reversed where mechanical power is converted to electrical power as denoted by (3.5)-(3.6).

$$P_{mech} = P_{conv} - P_f \tag{3.5}$$

$$P_{elec} = P_{conv} - P_{eL} \tag{3.6}$$

P_{conv} is the power converted to electricity, P_f is the mechanical power loss to friction, and P_{eL} is the electrical power loss due to internal motor resistance. Where each of these terms is defined as:

$$P_{mech} = T_e \omega_e \tag{3.7}$$

$$P_{conv} = T_{em} \omega_e \tag{3.8}$$

$$P_f = Q_f \omega_e \tag{3.9}$$

$$P_{eL} = Ri^2 \tag{3.10}$$

$$P_{elec} = Vi \tag{3.11}$$

Making use of Eq (3.2) in Eq. (3.6) and replacing $\dot{\theta}$ with ω_e, the output voltage (V) can be solved by combining equation Eq. (3.8), (3.10), and (3.11), into Eq. (3.6), which is shown by Eq (3.12). Considering that the motor torque constant K_t and back emf constant K_b are identical, we can see that the generator voltage production (V) is the negative of the motor voltage input. Thus, the governing equations of generator operation are fundamentally the same as a motor except the electrical potential, in essence, is run in reverse where all inputs to the generator are negative to signify the reverse operation, which essentially produces an opposing current for charging the battery.

$$V = K_b \omega_e - Ri - L\frac{di}{dt} \tag{3.12}$$

$$i = \frac{T_e - Q_f \omega_e K_t}{K_t} \tag{3.13}$$

Moreover, combining Eq. (3.7), (3.8), and (3.9) into Eq. (3.5) yields Eq. (3.13), which is the current production of the generator. For this study, the same model parameters as the motor model were used for the generator model. This was done considering that the generator and the motor are physically identical and simply operating in an inverse fashion to each other. The generator model uses a torque input to determine the rotational speed, voltage, current, and, ultimately, the

power output of the generator. Voltage and current are supplied to the battery model as inputs for charging operations.

3.1.3. Battery Model

Battery models can be found in literature in numerous forms varying in complexity, as shown in Figure 19. A battery model typically is used to model the battery performance in the development of various systems that require battery power or to control power distribution from the battery. Applications of battery models such as in simulating a battery management systems (BMS), micro-grid simulation, battery architecture optimization, and hybrid powertrain design all make use of some form of battery model to simulate aspects such as battery voltage supply and charging/discharging operations.

Models	Accuracy	Complexity	Physical interpretability	Suited application
Physical	Very high +++	High (> 50 parameters) –	High ++	Battery system design stage
Empirical	Medium -	Low (2–3 parameters) –	Low –	Predictions of life time and efficiency
Abstract	Medium -	Medium to low (from 2 up to 30) +	Limited to acceptable +	Real-time monitoring and diagnosis

Figure 19. Battery model classification [55]

As previously discussed in the motor model description, the fidelity or complexity of the model depends on the design requirements of your system. Thus, battery models are characterized into three categories: a physical or physics-based model, empirical or mathematical models, and abstract or equivalent circuit models, as defined in [55,56]. The physics-based models are low-level models with a high accuracy level. They describe the interaction of complex electrochemical phenomena occurring inside the cell, such as thermodynamics, active species kinetics, and transport phenomena [55]. The physics-based model is typically more computationally expensive

because it accurately models the electrochemical dynamics of the system using highly nonlinear equations [56]. Thus, it is not suited for high-level simulation where speed and accuracy are desired. The mathematical models can be classified into two different groups, which are analytical and stochastic models [56]. These models, however, are limited in terms of accuracy if the model is too simple but can be very accurate if a sufficiently complex model is chosen, unfortunately, at the cost of computational speed [55]. Finally, the abstract model class, which commonly utilizes the equivalent circuit model, is prevalent in the modeling community. Different equivalent circuit forms are possible, therefore providing flexibility in model development to achieve varying levels of model performance in terms of accuracy and speed. This is possible because circuit-based models are simple and practical because they allow for the complex electrochemical process to be replaced by a simple electrical circuit that preserves battery dynamics without degrading accuracy [55]. These equivalent circuit models do require the use of experimental data to develop lookup tables; however, the development effort is significantly less than the other two methods described. For this reason, the equivalent circuit model was used to develop the battery model in this work. However, the accuracy and speed of the model are dependent on the architecture of the equivalent circuit model one chooses to model.

$$\dot{V_1} = -\frac{V_1}{R_1 C_1} - \frac{1}{C_1} \tag{3.14}$$

$$\dot{V_2} = -\frac{V_2}{R_2 C_2} - \frac{1}{C_2} \tag{3.15}$$

$$SOC = SOC_0 + \int \frac{-I}{Q_c} \tag{3.16}$$

$$V_t = OCV + V_1 + V_2 - IR_o \tag{3.17}$$

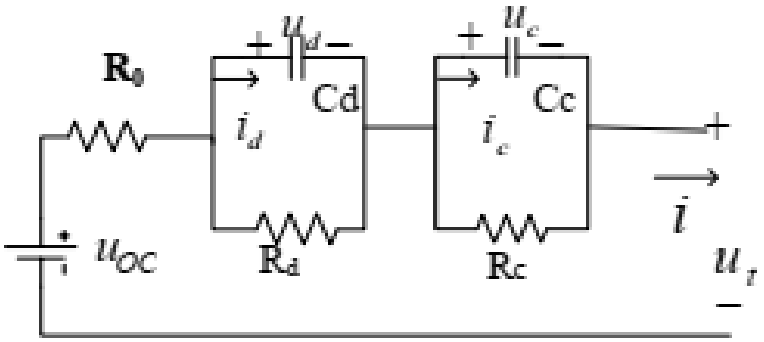

Figure 20. Equivalent circuit model diagram [57]

Within the equivalent circuit category of battery models, multiple forms of models exist, as defined in [58,59]; however, each model uses a form of a resistor or a capacitor to describe the dynamic behavior of the battery cell. The most common circuit mode is a resistor-capacitor network (RC), where a resistor and capacitor are connected in a way that describes the battery response curve. The order or the number of RC pairs can be manipulated in a way where the model accuracy can be very acceptable. The method used in this work utilized a second-order RC (2 RC) model shown in Figure 20, where two parallel RC networks are connected in series with a resistor to characterize the battery response better. Moreover, the findings of [57] show that the 2 RC model can better represent the battery response when compared to first-order models (1 RC), where the 1 RC model produced residuals up to 4.5 mV.

In comparison, the 2 RC model achieved residuals of 2.0 mV. The 2 RC model, as shown in [60], is just as accurate as higher 3 or 4 RC models, with the second-order model achieving approximately 1-2.5 mV at a SOC of 60%. In contrast, the higher-order models achieve 1 mV or less depending on the number of time constants or RC pairs. Thus, the 2 RC pair model was chosen because it offers acceptable accuracy in replicating the battery response, and simulation speed is reasonable because the model parameters are far less than those of higher-order models. The reduced number of parameters offered by the 2 RC model is essential because, as discussed later

in this section, these parameters will be populated into a lookup table (LUT), which can cause considerable increases in simulation time if populated with too many variables or too many LUTs are used in general. Moreover, the use of the 2 RC model simplifies the parametrization process, which is discussed later in this section. It also reduces the number of parameters that need to be optimized to provide model accuracy and stability.

$$V(t) = IR_1\left(1 - e^{-\frac{t_r}{\tau_1}}\right) + IR_2\left(1 - e^{-\frac{t_p}{\tau_2}}\right)\left(1 - e^{-\frac{t_r}{\tau_2}}\right) \tag{3.18}$$

$$\min_{(R_1,R_2,\tau_1,\tau_2)} f(R_1, R_2, \tau_1, \tau_2) = \sum_{i=0}^{N} (V_i(t) - \{(V\}_{data})_i)^2 \tag{3.19}$$

$$R_o = \frac{\triangle OCV}{I} \tag{3.20}$$

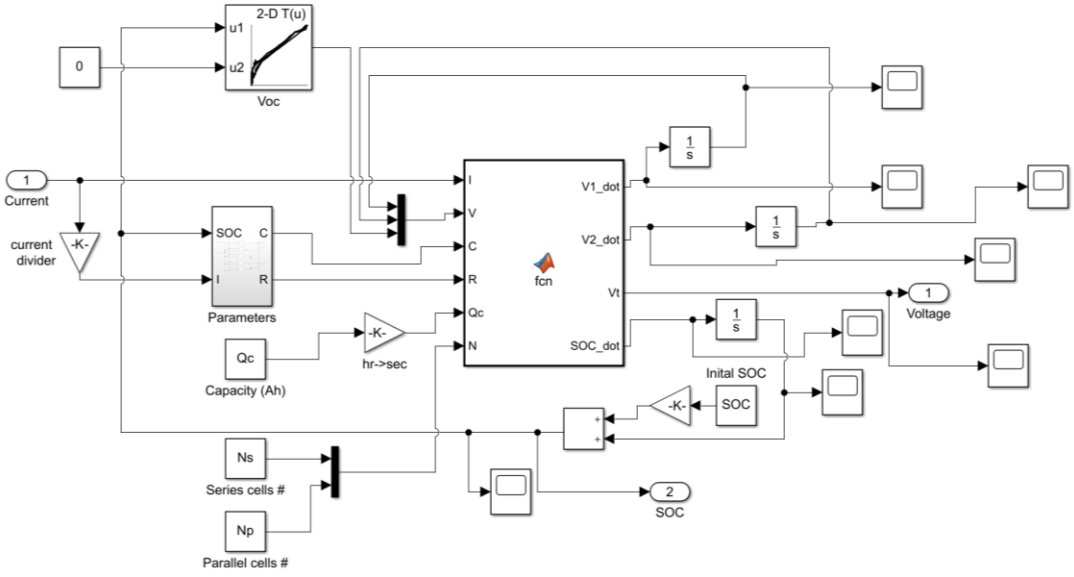

Figure 21. Battery Simulink model

The battery model (Figure 21) uses an input of current (as requested by the propulsion motor and generated by the generator model) and outputs battery voltage and the corresponding SOC. This model was developed using charge and discharge voltage and current data (Figure 22) for a Sony VTC6 18650 lithium-ion cell with a nominal voltage of 3.6 V and a maximum capacity of 3 Ah.

The battery data contained charge and discharge rate for 0.5 C, 1 C, and 2 C and was provided by researchers at the Air Force Research laboratory (AFRL). The model is characterized by Eq. (3.14)-(3.17), representing the mathematical model for a 2 RC pair equivalent circuit model.

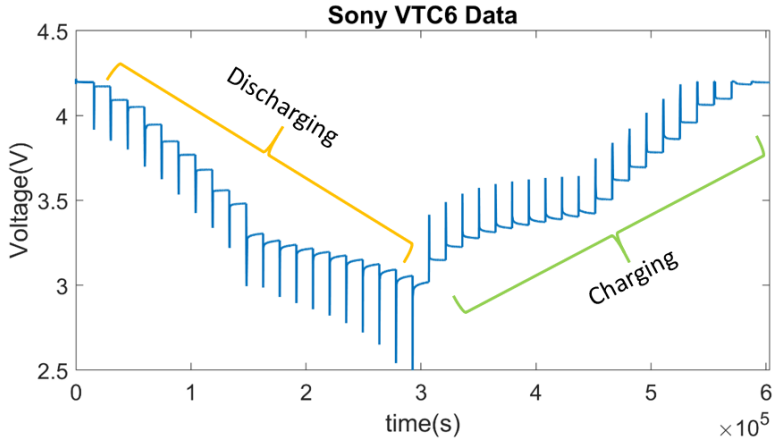

Figure 22. Sony VTC6 charge/discharge data

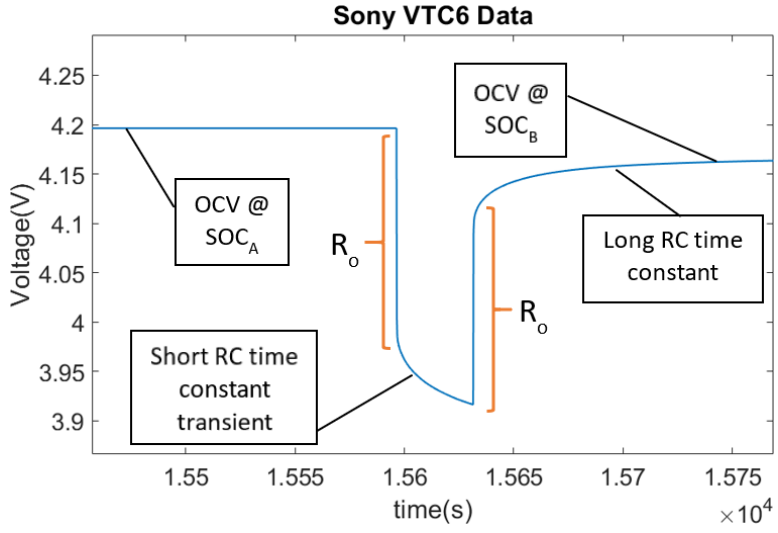

Figure 23. Battery response curve

Model parameters were calculated using Eq. (3.18), which was adapted from [61] and is an approximate curve fit that represents the transient discharge or charge curves of a Li-Ion battery, as shown in Figure 23. This equation is composed of 6 parameters that must be defined, which are R_1, R_2, tr, tp,τ_1, and τ_2 where R1 and R2 are the resistance of the first and second RC pair,

respectively; tr and tp are the duration of the pulse and relaxation transient duration time; and τ_1 and τ_2 are the time constants for the pulse and relaxation transient phase, respectively. These parameters define the shape of the transient response curve and must be optimized to provide the proper fit for the test data. Thus, an offline optimization routine was developed to loop through the discharge and charge curves shown in Figure 22, which each correspond to a different SOC. The optimization routine created in MATLAB utilized the least-squares method (Eq. (3.18)). The optimization parameters R_1, R_2, τ_1, and τ_2, were optimized to best fit the test data for the relaxation curve or Long RC time constant transient of the battery. This optimization was then repeated for each SOC curve and each C rate data set where a LUT of the model parameter R_1, R_2, C_1, and C_2 was then created, which was adapted from [62].

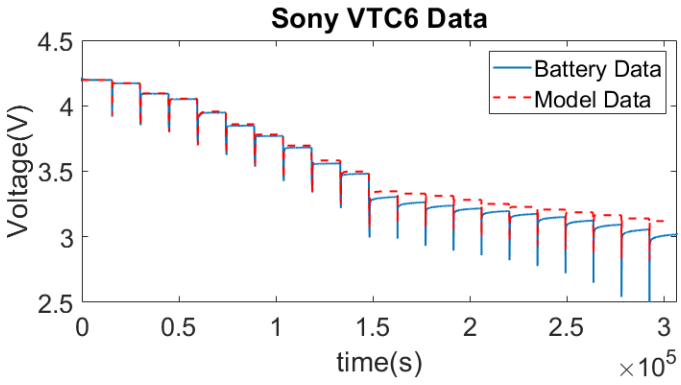

Figure 24. Battery model response 1C discharge cycle

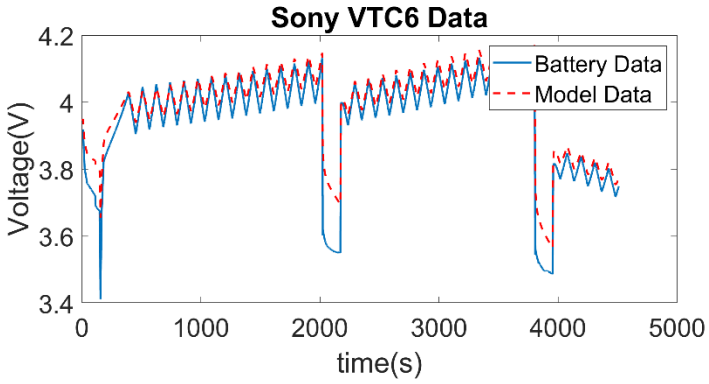

Figure 25. Battery model response random charge/discharge profile

The optimization process requires initial guesses for R_1, R_2, tr, tp, τ_1, and τ_2 values, which can affect the results of the optimization. This means that the accuracy of the model parameters is very sensitive to these six parameters in Eq. (3.18). In a study on the global sensitivity of 2 RC equivalent circuit model parameters [63], the sensitivity analysis demonstrated that the output of the second-order RC model is most sensitive to the series resistance Rs in the model (Figure 20) and the τ_2 term in Eq. (3.18).

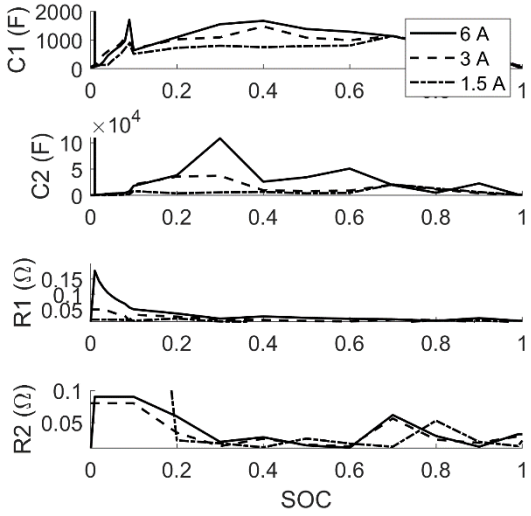

Figure 26. Battery model parameters for charging data

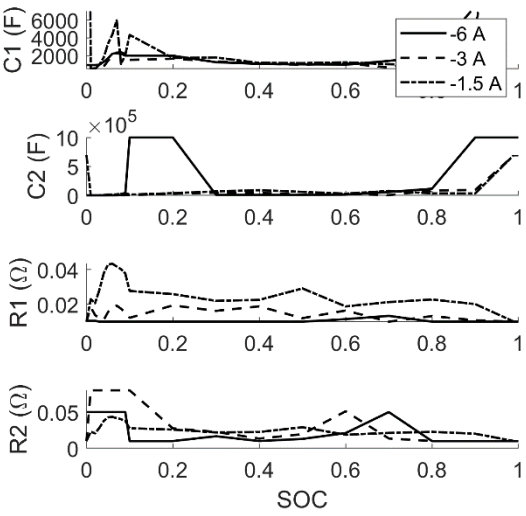

Figure 27. Battery model parameters for discharge data

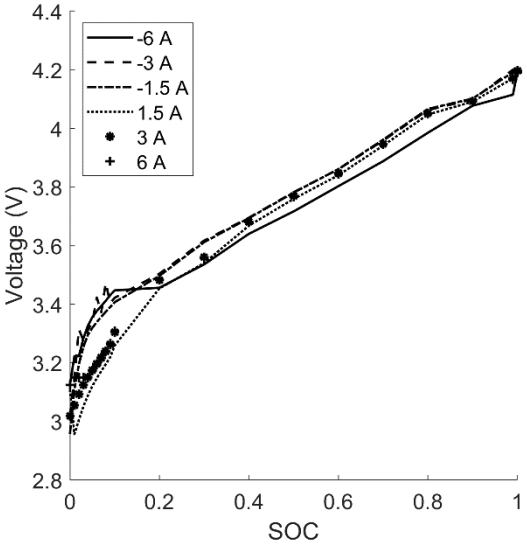

Figure 28. Battery model voltage parameters

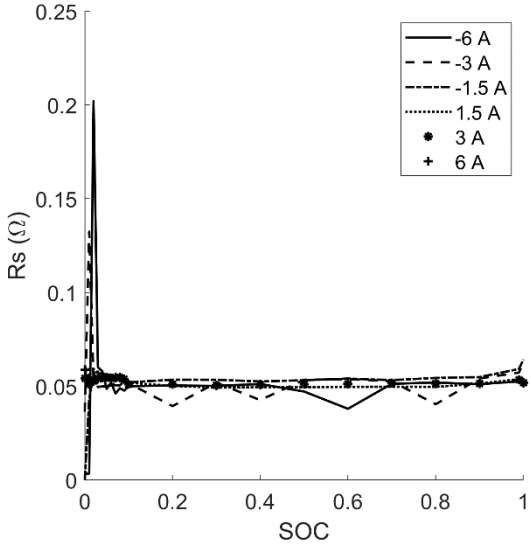

Figure 29. Battery model series resistance parameters

Thus, the other terms in the Eq. (3.18) can be set as constants once suitable values are determined. The optimization now relies only on varying the R_s and τ_2 until optimal results are achieved. However, the Rs values are directly determined from the response curve, as shown in (Figure 23). The R_s values have less uncertainty than the τ_2 value and, as a result, were not varied in this analysis. Since the optimization is highly sensitive to the initial guess of the τ_2 variable, the routine could easily converge to a local minimum where sub-optimal solutions exist rather than a global minimum. Therefore, the optimization was repeated, and then τ_2 was tuned until model parameters were found that provided good agreement of the battery model with the battery test data. The model parameters calculated by the optimization for both the charge and discharge data are shown in Figure 26 – Figure 29 for the RC pair parameters, OCV, and series resistance values. The results of Figure 24 and Figure 25 shows the model response compared to the actual battery discharge/charge data for a 1C discharge cycle as well as a random charge/discharge profile.

3.1.4. Engine Model

The engine model (Figure 30) uses a throttle and speed input from the engine throttle controller and the generator, respectively. These inputs determine the torque output from the engine, which is constructed using a LUT for power and BSFC (Brake Specific Fuel Consumption) as a function of engine speed at different throttle settings. The LUT for engine performance was generated through dynamometer testing of the 3W-28i engine, which is a single-cylinder, 2-stroke, carbureted gasoline engine used in many small Group 2 UAS.

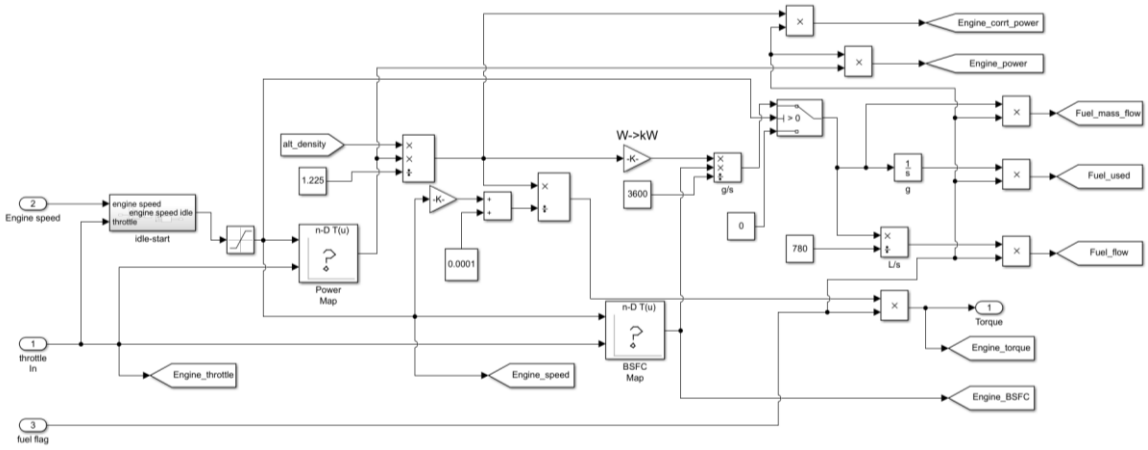

Figure 30. IC engine Simulink model

The use of an engine map generated from test data is a defining feature of this work. This overcomes limitations posed by a lack of detail in manufacturer-supplied data, which is also subject to significant uncertainty. Further, given the significant impact of engine efficiency (or BSFC) on aircraft range (Eq. (2.1)), and its variation over the operating range of the engine, it is critical to consider the complete engine map while developing an appropriate powertrain control strategy. Moreover, given the considerable differences in the architecture and operation of small two-stroke engines used in the UAS, as compared to conventional scale IC engines, there is a lack of confidence in the accuracy of standard mean values mathematical [64] or physics-based [65] engine simulation models in lieu of having actual engine test data. The engine model also includes a fuel metering

aspect or "fuel tank," which is depleted during the mission, with the torque output forced to be zero when the fuel tank is detected to be empty. The model includes a power correction factor based on altitude air density provided by the mission profile block shown in Figure 30, which scales the power output using the ratio of air density at altitude to the sea level air density. The power correction factor is used to simulate the engine power reduction observed when combustion engines operate at altitudes with lower air density.

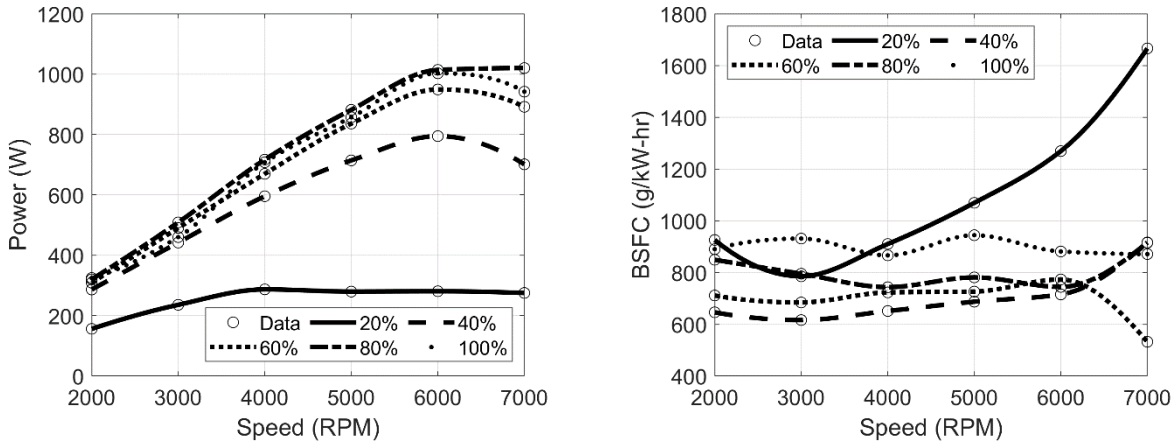

Figure 31. 3w-28i Performance Data

3.1.5. UAS Aircraft Model

The aircraft dynamics model (Figure 32) used in this analysis is a simple point mass approximation (Figure 33) that analyzes the sum of the forces acting on the aircraft. The model uses the thrust input from the propeller model to calculate the airspeed of the aircraft. Eq. (3.21) — (3.25) describe the vertical and horizontal forces on the aircraft used in the model.

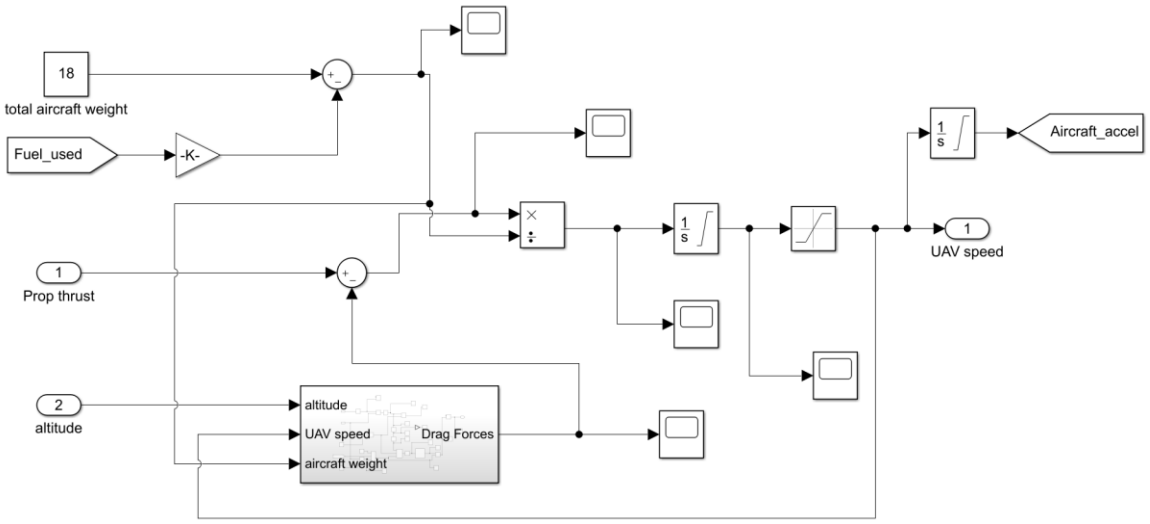

Figure 32. UAS aircraft Simulink model

The model calculates the aircraft speed based on the thrust input. It then uses the speed and altitude information from the flight profile to calculate the flight angle. The flight angle allows for calculating the coefficient of lift, which is then used to determine the coefficient of drag using a LUT for the lift-drag polar. The model in this simulation uses an aircraft weight of 18 kg, which is equivalent to a group 2 UAS aircraft, and the data for the lift-drag polar (Figure 34) for the AAI Aerosonde UAV. The parameters used in Table 2 were also used in the model to define geometric parameters such as wing area to facilitate lift and drag calculations.

Table 2. AAI Aerosonde parameters

CD_0	CL_{min}	Oswald coefficient	Wingspan	Wing area
0.0434	0.23	0.75	2.89	0.55

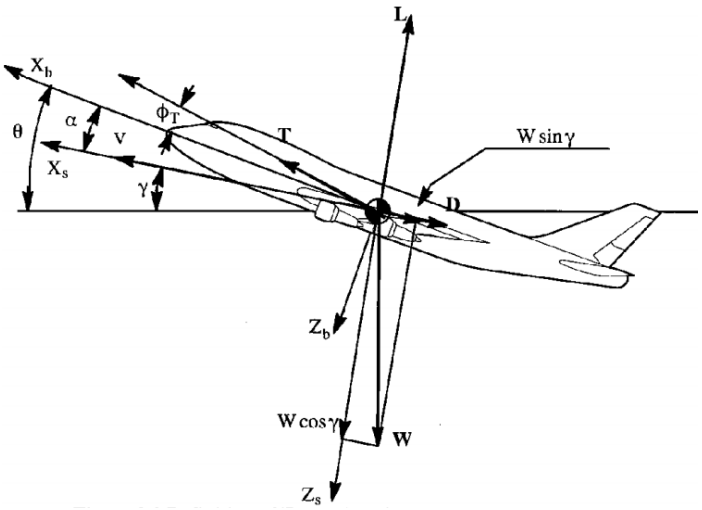

Figure 33. Aircraft point mass model [66]

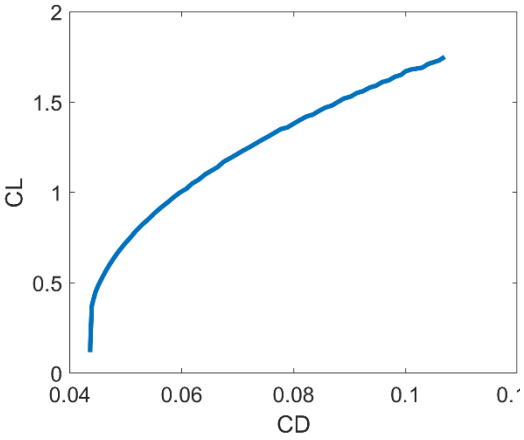

Figure 34. Aircraft model lift/drag polar

$$T\sin\theta - D\sin\theta + L\cos\theta - W = m\frac{dV_v}{dt} \tag{3.21}$$

$$T\cos\theta - D\cos\theta - L\sin\theta = m\frac{dV_h}{dt} \tag{3.22}$$

$$C_l = \frac{L}{\frac{1}{2}\rho S_w V^2} \tag{3.23}$$

$$C_d = \frac{D}{\frac{1}{2}\rho S_w V^2} \tag{3.24}$$

$$\dot{h} = V\sin\theta \tag{3.25}$$

3.1.6. Propeller Model

The propeller model (Figure 35) uses inputs of motor speed and aircraft speed to calculate the advance ratio *J* of the propeller (Eq. (3.26)), which is then used as input to a lookup table for thrust and power coefficients. The data for thrust and power coefficients were obtained from the APC propeller database for a 20x10 propeller [67].

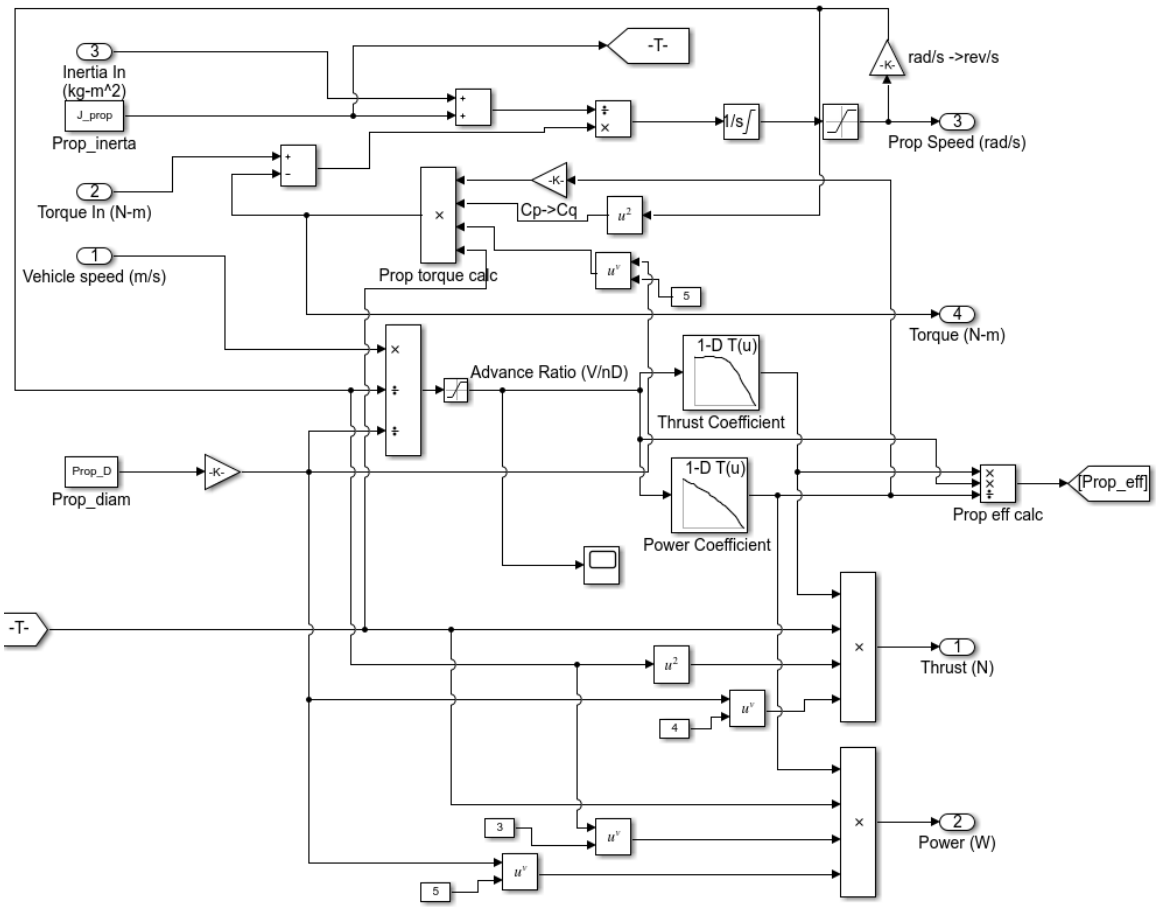

Figure 35. Propeller Simulink model

These coefficients are then used in Eq. (3.27) — (3.30) to calculate the thrust, power, and torque that the propeller requires for a given flight speed and torque input from the propulsive motor. The output of the model is thrust, which is used later in the aircraft dynamics model to determine the aircraft speed.

$$J = \frac{V}{nD} \tag{3.26}$$

$$C_Q = \frac{C_p}{2\pi} \tag{3.27}$$

$$C_T = \frac{T}{\rho n^2 D^4} \tag{3.28}$$

$$C_P = \frac{P}{\rho n^3 D^5} \tag{3.29}$$

$$C_Q = \frac{Q}{\rho n^2 D^5} = \frac{C_p}{2\pi} \tag{3.30}$$

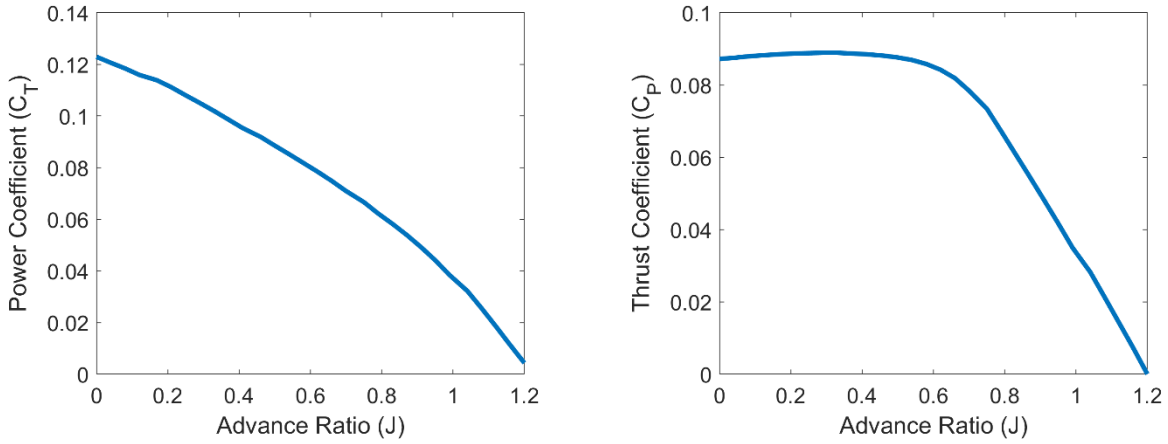

Figure 36. Propeller model data

3.2. Mission Simulation/Flight Profile

Three different flight profiles are used to simulate different operating scenarios, including cruising flight, with and without maneuvers, and a surveillance mission. The mission profile comprises a speed and altitude profile that characterizes the aircraft's operation for a 30-minute flight time. The first profile shown in Figure 37a is for a straightforward climb to a cruise phase followed by a descent and landing phase. This simple profile represents a scenario where power demand remains constant during cruise at a speed of 30 m/s at an altitude of 2500 m.

The second profile simulates a scenario where the aircraft will perform some maneuvers at an altitude of 2500 m. This profile has some speed changes where the aircraft accelerates and decelerates to different speeds, as shown in Figure 37b. The last profile shown in Figure 37c is used to simulate a surveillance mission. For the surveillance profile, the aircraft takes off and climbs to the cruise phase, after which it ascends to a higher altitude for the surveillance segment at a lower

speed and finally climbs to the aircraft's maximum altitude of 3000 m at the maximum aircraft speed of 40 m/s.

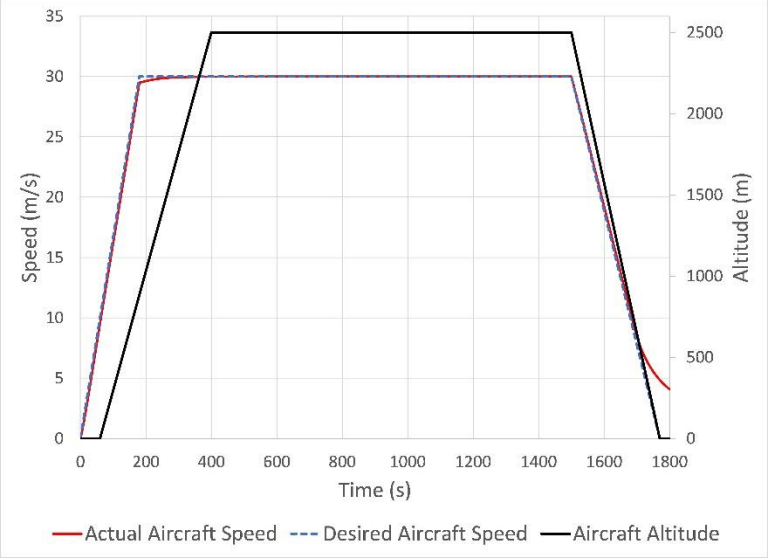

(a)

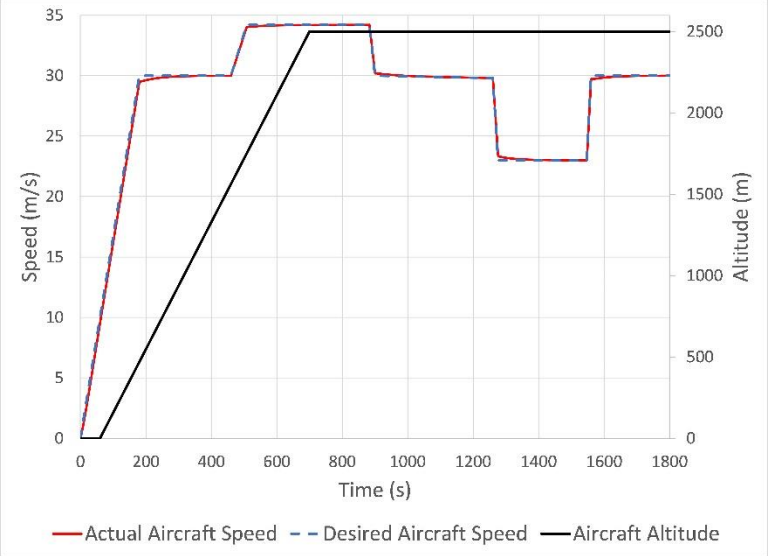

(b)

(fig. cont'd.)

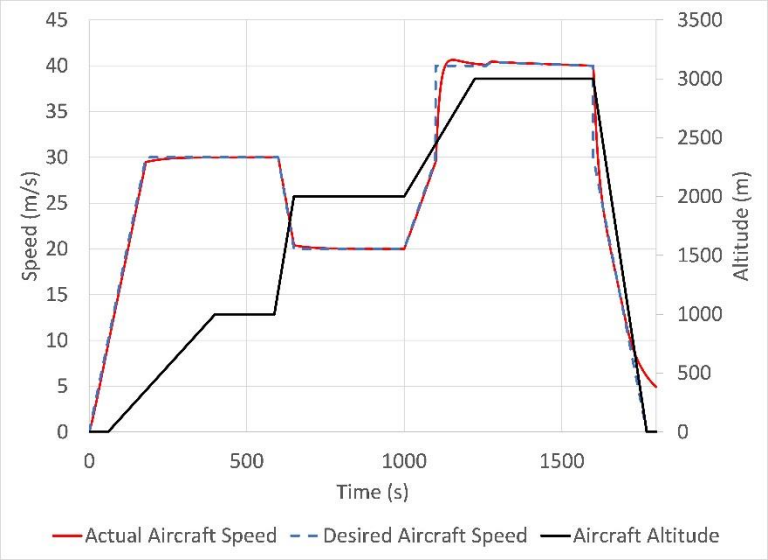

(c)

Figure 37. Simulation flight profiles: (a) Cruising profile; (b) Maneuver profile; (c) Surveillance profile

The data set labeled as actual aircraft speed shows the aircraft speed predicted by the powertrain simulations, whose results will be described in detail in the following section. These flight profiles are used to assess the change in propulsive power demand of the aircraft and subsequent effects on the power requested from the engine-generator system. As the propulsive power demand increases and battery SOC becomes low, the engine-generator must increase its power production, leading to increased fuel usage. This power increase is observed going from the cruising to the maneuvering to the surveillance profile. The highest power levels are observed for the surveillance profile since the aircraft is commanded to climb to a higher altitude at maximum speed. Likewise, the maneuvering flight profile is seen to have a higher power requirement than the simple cruise profile.

Chapter 4. Series HEUAS Control Methods

4.1. Baseline Control

The control logic is a key component of the HEUAS powertrain, whose goal is to supply the required propulsive power during the mission profile for the UAS. Thus the function is to provide electrical power to maintain the desired battery SOC while minimizing fuel usage to maximize aircraft range and endurance. Three different control strategies are employed in this work to analyze the effect on the fuel consumption of the hybrid powertrain.

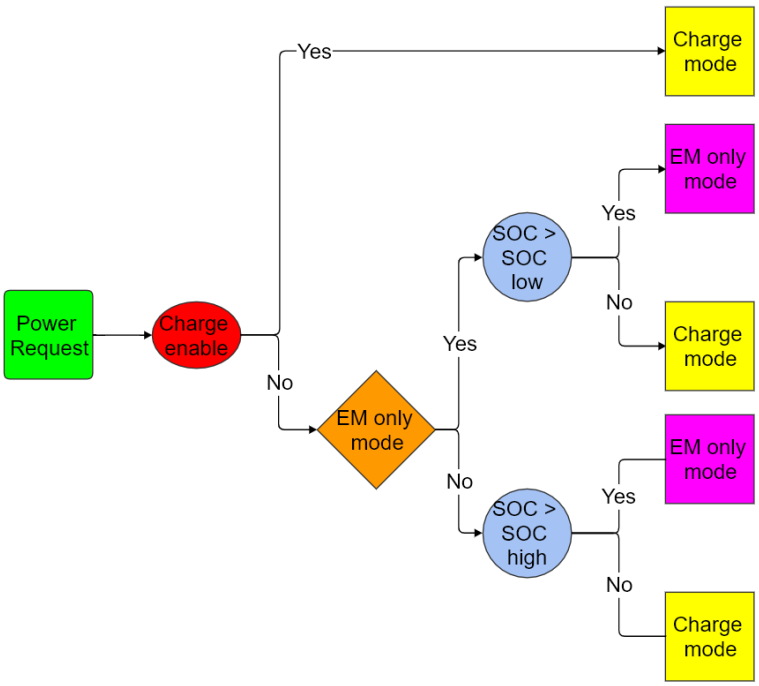

Figure 38. Charge enable control logic

The first control scheme was a baseline power follower form of control adapted from [46], which controlled the charging operation by maintaining the battery SOC within a 75-95% range based upon the power requested for system operation and charging shown in Figure 38. Since the power requested from the IC engine and generator can vary during flight, the power requirements can change depending on the flight profile. The SOC range chosen in this scheme corresponds to the range with the lowest ohmic resistance for the battery, which corresponds to the most efficient

range of operation of the battery. This control method served as a baseline because it is the simplest method of control and because it is the least efficient method of controlling the ICE during charging because the engine can possibly operate in an inefficient region while attempting to maintain the battery SOC, thus increasing fuel consumption. This control scheme functions by controlling the engine throttle to maintain the generator power output to provide sufficient propulsive power for flight and excess power to charge the battery when its SOC falls below the set threshold. Excess power corresponds to the power required to charge the battery at a 1C rate, where the SOC is maintained within previously mentioned set bounds.

4.2. IOL Control

The Ideal Operation Line (IOL) control strategy, also known as the Optimal Operation Line (OOL) approach, for the series hybrid system is depicted in Figure 39 and forms the second control strategy used in this work. This control strategy prioritizes minimum fuel consumption from the engine through a pre-determined operating line adapted from [68]. The IOL strategy functions by tracking the minimum BSFC operation line shown in Figure 40. This line is obtained by finding the maximum torque at the minimum BSFC on different constant power lines for steady-state conditions. This method enables the engine to operate in its optimal efficiency region of maximum torque at the lowest BSFC, thus minimizing fuel usage.

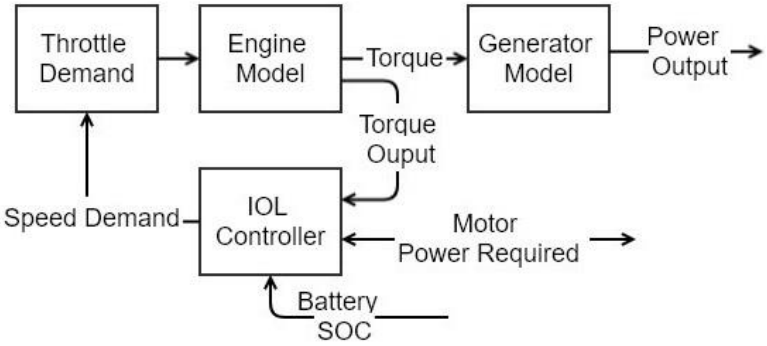

Figure 39. IOL control scheme

The IOL for an engine requires a detailed BSFC map of the engine. Once acquired, lines of constant power are overlaid on the engine map, which is populated with iso-contours of BSFC. Each line of constant power intersects multiple contour lines of constant BSFC and also various points on the same BSFC iso-contour. The set of intersection points with the lowest BSFC iso-contour are found, and among those points, the one with the highest torque is chosen as the ideal operating point at that power level. After connecting these points on all the constant power lines, the IOL is created. Using this method for finding the IOL and the test data for the 3w-28i (Figure 31), the IOL line used in this work was found and is shown in Figure 15. The lines of constant power overlaid on the BSFC map in Figure 40 range from 315 W to 990 W in Figure 40.

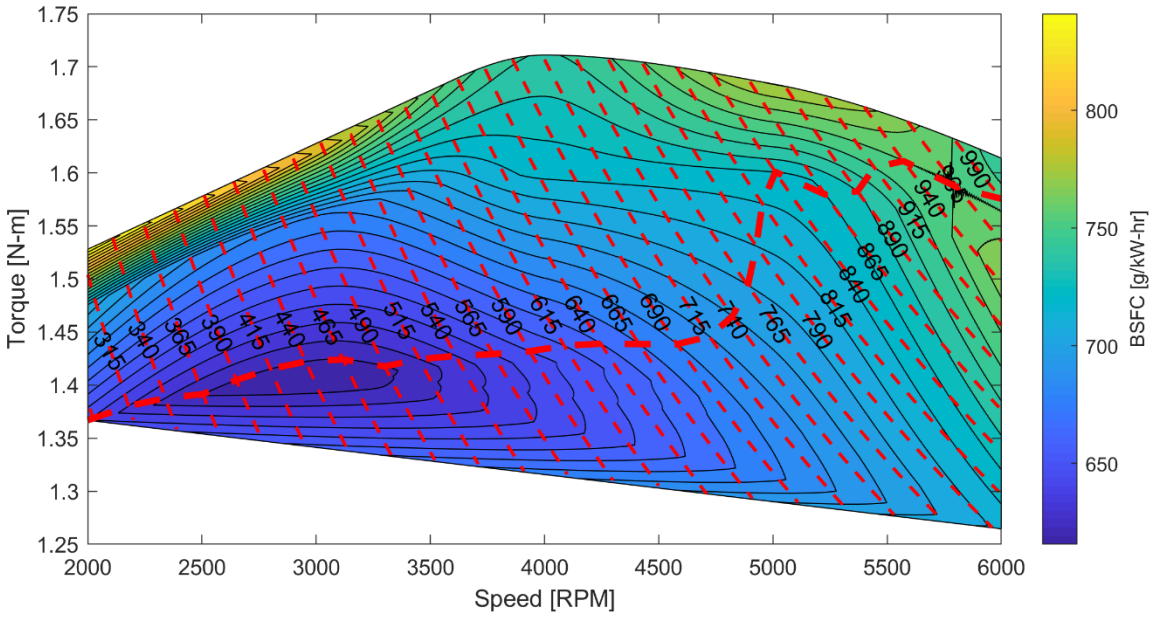

Figure 40. Engine efficiency contour map and ideal operating line

The implementation of the IOL controller starts with a lookup table of the IOL to serve as a reference signal for the engine torque based on the power requested by the HEUAS system. This torque is then used to reference the speed that the engine should be operating at to possibly achieve an operating condition at the minimum BSFC. This torque request is then used as a throttle command, which is sent to the engine model to regulate the engine operation. The control loop will

regulate the torque to the ideal operating torque using a PID controller and its corresponding speed, which should force the engine to operate in its most efficient region and provide enough power for charging operation. The IOL controller is activated similarly to the baseline scheme where the controller is activated when the SOC falls below 75%, and engine torque or power is regulated to provide the necessary power to charge the battery at a 1C rate to maintained the SOC within a boundary of 75% to 95%. With respect to implementation, the critical difference between the two control schemes is the ability of the IOL approach to find the IC engine operation point with the lowest BSFC for the given power requirement. The baseline control logic also generates the requested power, but without any consideration of engine BSFC.

4.3. Fuzzy Logic Control

The last control method explored is fuzzy logic rule-based control (FLC), which uses multivalued logic. The fuzzy controller (Figure 41) uses the linguistic representation of the control inputs, which is converted into a numerical representation with membership functions in the fuzzification and defuzzification process [38]. The advantage of using the fuzzy controller is the increased degrees of freedom of control, meaning more variables in the system such as the SOC, generator power, and engine efficiency can now be optimized to operate within their most efficient region. This degree of control enables the powertrain system to operate at its optimal efficiency, reducing fuel consumption and increased range.

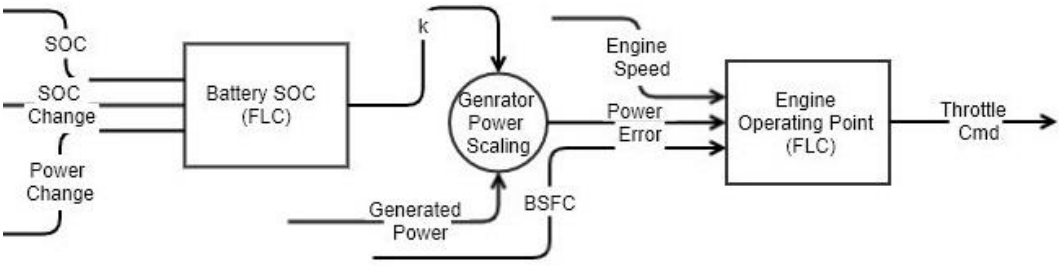

Figure 41. Fuzzy logic control diagram

The controller functions by utilizing two FLC's where one determines the generator demand to maintain the SOC within a nominal range. The second manages the engine operation to minimize generator power demand error while reducing engine fuel consumption. The control method was adapted from [49], where a power scaling factor (k) is used to determine the amount of generator power that should be supplied based upon a reference power value. The reference power is determined based upon the maximum power output of the generator, which is 1000 W. The scaled generator power is then compared to the current generator power to produce an effort signal used in the engine operating point FLC.

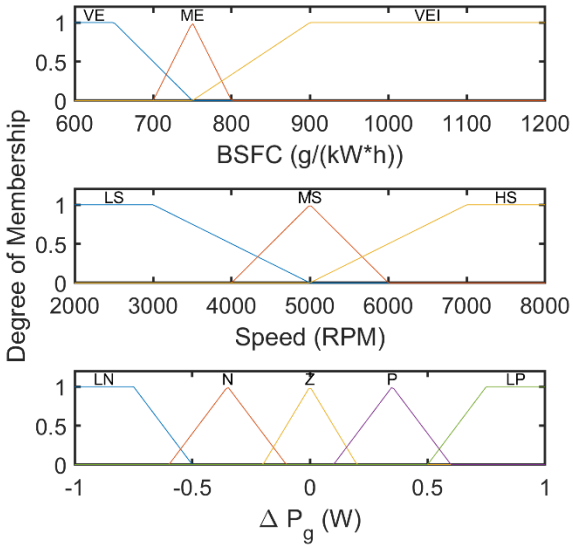

Figure 42. FLC1 input membership functions

The engine operating point FLC then uses fuel consumption and engine speed data to determine the proper throttle setting to minimize fuel consumption. The FLC also requires a set of membership functions and rules to determine the relationship between the input variables to the output variable to produce the required performance. These membership functions (Figure 42, Figure 43) define the range of operation for the system and their classification within the rule-set (Table 3, Table 4).

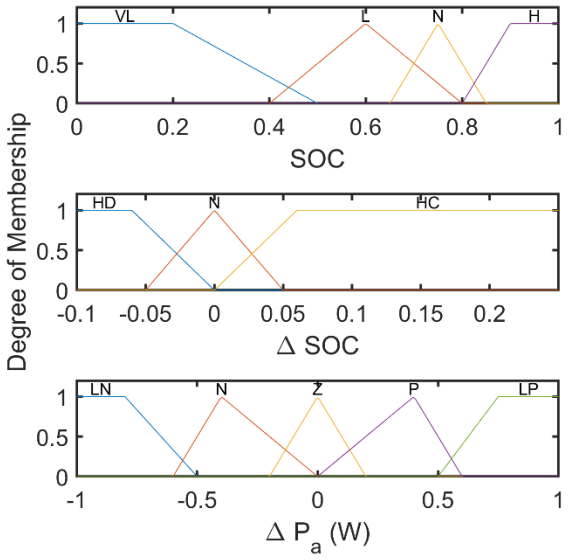

Figure 43. FLC2 input membership functions

Three different rules exist for each FLC controller. The first controller (FLC1) responsible for determining generator demand uses the SOC, ΔSOC, and the change in power available (ΔPa) to determine the scaling factor for generator power production. The second controller (FLC2) utilizes the engine speed, instantaneous BSFC, and the generator power error (ΔPg) to determine the amount of throttle that should be requested to produce the desired amount of generator power at the lowest BSFC value. These membership functions then require a set of rules which define the desired operation of the controller. The rules defined in Table 3 and Table 4 define the rules for both FLC1 and FLC2, respectively. These rules aim to operate the engine in the low to moderate throttle range where efficiency is high, as shown in Figure 31. The results of these three control schemes will be compared to determine the level of fuel savings that can be achieved for specific missions described in the next section.

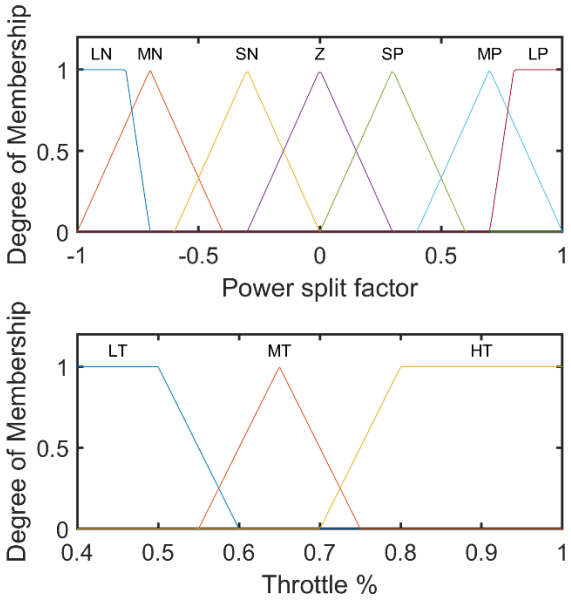

Figure 44. Output membership functions

Table 3. Rule set for FLC1

	Very low SOC				
(ΔSOC)/(ΔPa)	LP	P	Z	N	LN
HD	SP	SP	MP	LP	LP
N	SP	SP	SP	LP	LP
HC	SP	SP	SP	LP	LP
	Low SOC				
(ΔSOC)/(ΔPa)	LP	P	Z	N	LN
HD	SP	SP	SP	SP	MP
N	SP	SP	SP	SP	MP
HC	SP	SP	SP	SP	SP
	Nominal SOC				
(ΔSOC)/(ΔPa)	LP	P	Z	N	LN
HD	SN	SN	Z	SP	SP
N	MN	SN	Z	Z	SP
HC	MN	SN	Z	Z	SP
	High SOC				
(ΔSOC)/(ΔPa)	LP	P	Z	N	LN
HD	LN	MN	MN	MN	MN
N	LN	MN	MN	MN	MN
HC	LN	LN	MN	MN	MN

HD-High Discharge, N-Nominal, HC-High Charge
LP-Large positive, P-Positive, Z-Zero, N-Negative, LN-Large negative
MP-Moderately Positive, MN-Moderately Negative

Table 4. Rule set for FLC2

	Low BSFC				
(Speed)/(ΔPg)	LP	P	Z	N	LN
LS	MT	MT	MT	LT	LT
MS	MT	MT	LT	LT	LT
HS	MT	MT	LT	LT	LT
	Moderate BSFC				
(Speed)/(ΔPg)	LP	P	Z	N	LN
LS	HT	MT	MT	LT	LT
MS	MT	MT	LT	LT	LT
HS	MT	LT	LT	LT	LT
	High BSFC				
(Speed)/(ΔPg)	LP	P	Z	N	LN
LS	HT	MT	MT	LT	LT
MS	HT	MT	MT	LT	LT
HS	HT	MT	LT	LT	LT

LS-Low speed, MS-Moderate speed, HS-High speed
LP-Large positive, P-Positive, Z-Zero, N-Negative, LN-Large negative
LT-Large throttle, MT-Moderate throttle, HT-High throttle

Chapter 5. Results and Discussion

5.1. Mission Comparison

5.1.1. Cruising mission

The results of the simulation in terms of the propulsion motor response are relatively the same for each controller in each mission scenario. This results from the series hybrid configuration propulsion motor functioning independently from the engine-generator unit. Also, each control strategy focuses on operating the engine and has no effect on the motor's performance except when the battery SOC falls too low, and battery power capacity decreases and is not able to supply the power required to maintain flight speed. Therefore the results for the motor will be analyzed by mission rather than by control strategy.

For the cruising mission, the results in Figure 45 show the model response for the 30 min mission. Figure 45a shows the voltage and currents data where the motor current draw reaches nearly 40 A around the 400s range, which is when the aircraft is going through the climb phase of flight. After that period, the aircraft begins the cruising phase at the 500s point, which lasts for 1000s. We also observe that during the climbing phase, the motor speed (Figure 45b) reaches 850 rad/s (8100 rpm), which is close to the maximum speed of the KDE motor modeled in this work. In addition, the motor torque output reaches 2.8 Nm, which corresponds to the force required to accelerate the propeller to a speed that produces the required thrust.

Lastly, Figure 45c shows the motor power, which peaked at 2500 W during the climbing phase and then reduced to 500 W during the cruising phase. These results are representative of what an aircraft would experience during flight, where high power would be experienced during a climb. This same behavior is repeated for the other mission where power draw increases during times where aircraft speeds are high and the aircraft is climbing.

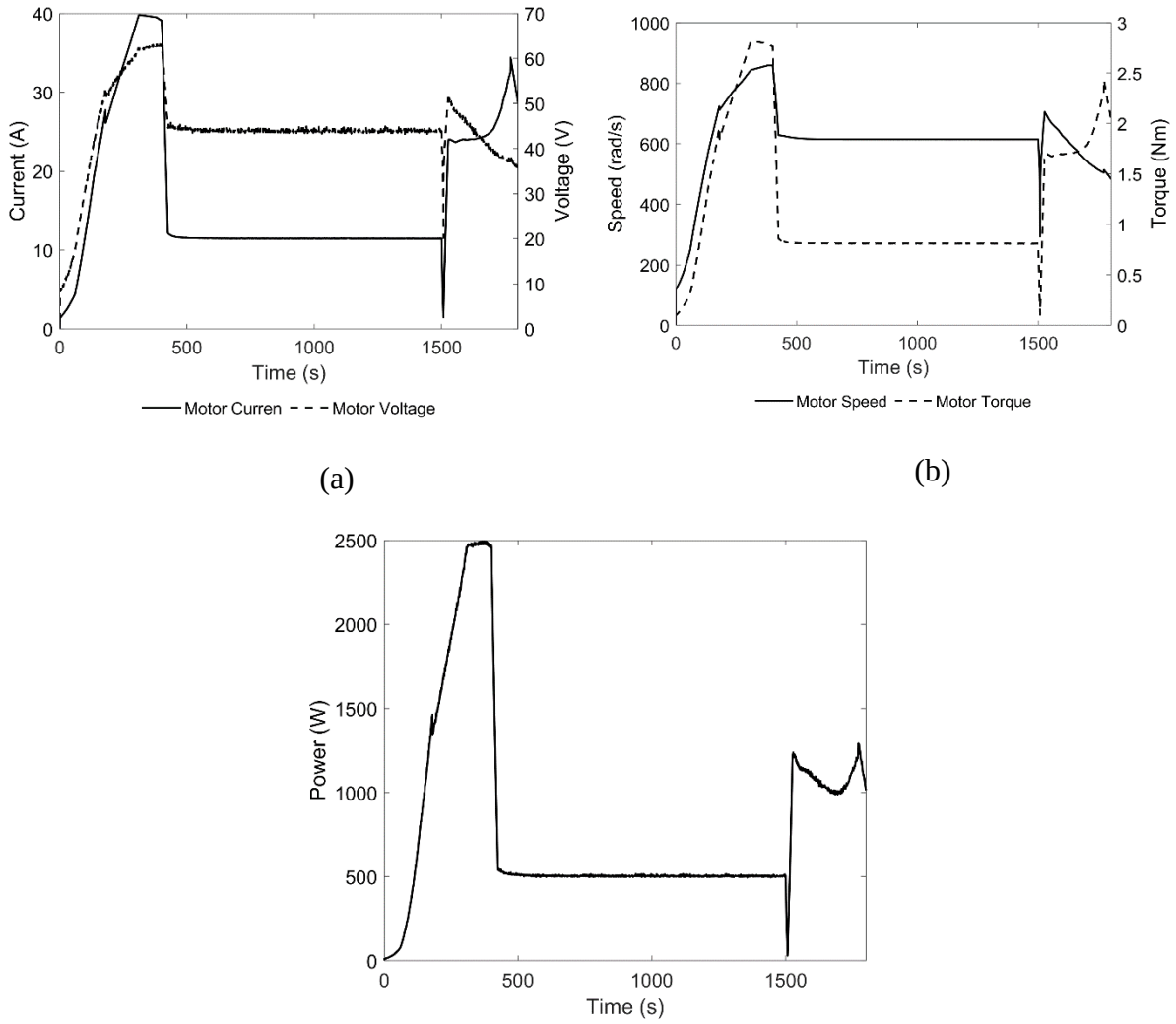

Figure 45. Cruising mission propulsion motor simulation data

5.1.2. Maneuvering Mission

The maneuvering mission results in Figure 46 demonstrate a similar trend where the climbing phase of flight has the highest voltage and current (Figure 46a) over the 30 min mission. The simulation shows that the current draw reached less than 30 A, which is less than that of the cruising mission. We also see that the response behavior closely matches the mission profile where the propulsion motor and torque all correspond to the changes in aircraft speed, which are used to simulate in air maneuvers where the aircraft changes speed while at cruise altitude.

The power profile in Figure 46c shows that the motor power peaked at 1600 W during the climbing phase, where the aircraft speed increased to 35 m/s. after this climbing phase, the power decreases to approximately 700 W at the 800-900s range where the aircraft is still traveling at 35 m/s. The power then further reduces to 500 W and then 300 W as the speed drops to 30 m/s and 23 m/s, respectively. These power variations are used to analyze the effect it would have on charging operations during the flight.

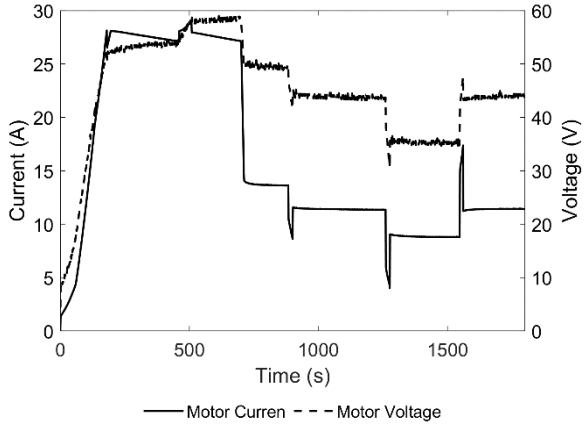

(a)

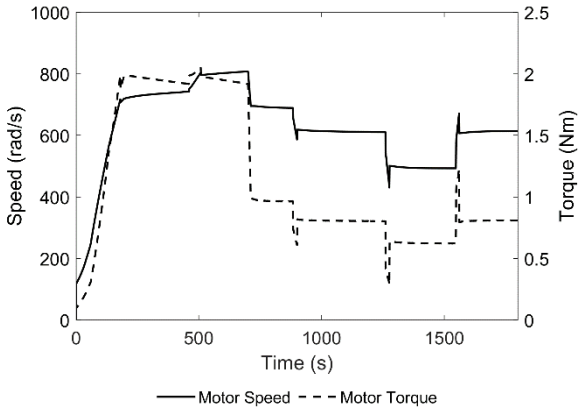

(b)

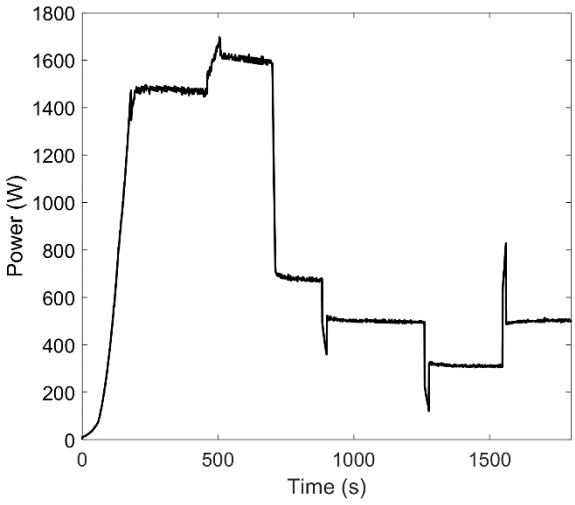

(c)

Figure 46. Maneuvering mission propulsion motor simulation data

5.1.3. Surveillance Mission

Lastly, the survalence mission was developed to test powertrain performance in a typical task that UAVs will be performing. In this profile, a phase was added where the aircraft climbs to a higher altitude at a lower speed to represent the surveillance phase of the mission profile. Following the surveillance phase, the aircraft undergoes another phase labeled the evasion phase, where the aircraft climbs to the maximum altitude of 3000 m at a maximum speed of 40 m/s. We should expect that during the evasion phase, the power demand should increase as the aircraft undergoes this phase of flight.

As we can see in Figure 47c, the expected response is observed. The aircraft demonstrated higher power draw during the climbing phase from 200-400s of approximately 1200 W, which is a similar finding of the other two mission profiles. We then see that dring the evasion phase at the 1100s mark, the power spikes to nearly 2500 W when the aircraft speed is commanded to 40 m/s. As the aircraft begins to settle into the climbing portion of the evasion phase, the power then settles to 1800 W and then further settles to approximately 1000 W as the aircraft travels at 40 m/s at a 3000 m altitude.

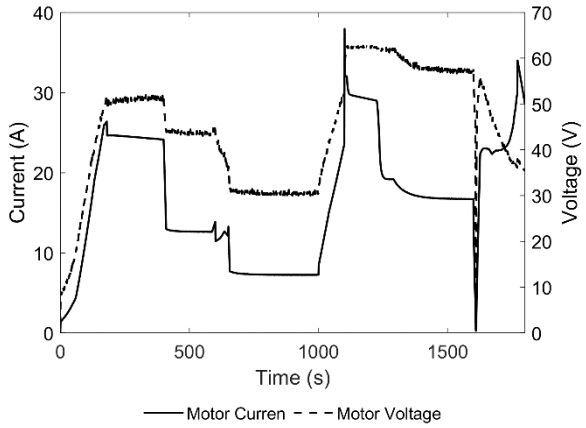

(a)

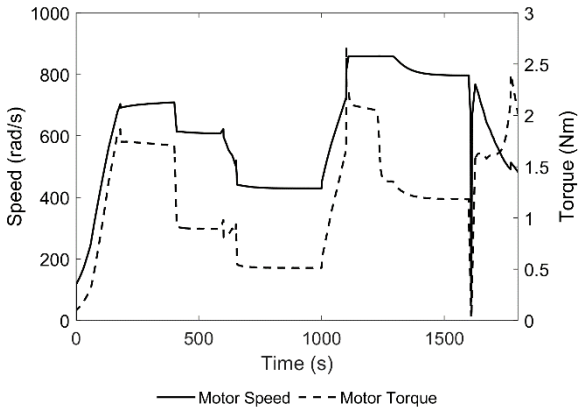

(b)

(fig. cont'd.)

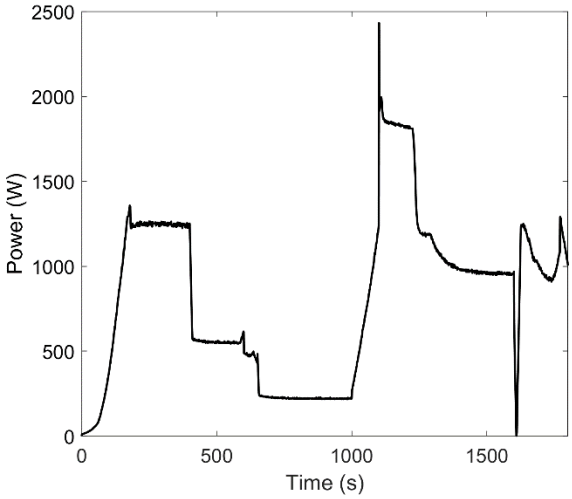

(c)

Figure 47. Surveillance mission propulsion motor simulation data

We can see that for each of these missions, the current draw never really exceeds 40 A. However, the maximum power observed among all the missions was 2500 W in the cruising mission. This result was not expected because the cruising profile was created to be the least intensive profile in terms of power consumption. However, an aircraft experiences high power may draw during climbing because the climbing segment is shorter than the other two missions, and the altitude that it is climbing to is relatively high. Nevertheless, results during the climb as expected, and the power draw did reduce drastically after the climbing phase in Figure 47c for the cruising profile. However, these results do not give direct insight into the model variables affected by the powertrain controller. These results merely give an insight into what power could be demanded during power generation.

5.2. Baseline Control Results

As mentioned in the previous section, the results of the propulsion motor will be the same for each mission, regardless of the control method used. However, the results of the SOC, fuel usage, and generator power, and current production are not similar among the various profiles. These aspects of the powertrain performance are directly affected by the three controllers

implemented in this analysis. Comparing the results for each mission profile based on the performed of each controller, we can gain a better understanding of the performance of the controllers.

The baseline controller produces roughly the same current during charging, as shown in Figure 48, where the current varies between 37 A to 42 A. This behavior is observed because the current drawn by the motor never really exceeds 40 A during each mission. However, we see that the current response curves are out of sync because the point at which the SOC reaches the charge sustaining mode of operation is achieved at different times because of how the motor current draw occurs in each mission.

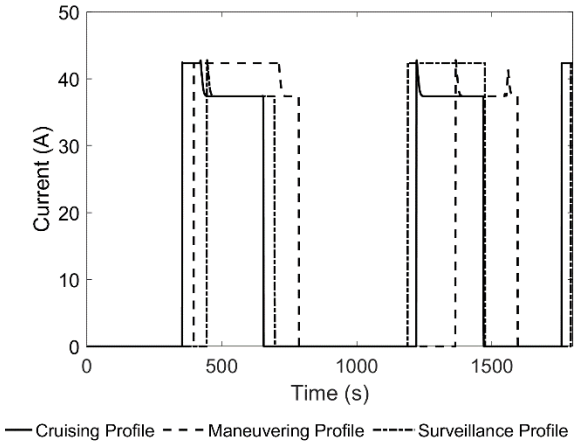

Figure 48. Baseline controller generator current

Moreover, we do see that for the maneuvering and surveillance profile, the points of peak power production do occur when undergoing periods of high demand. These periods occur, as previously discussed, during climbing for the maneuvering profile and during the evasion phase of the surveillance profile, which occurs at 500-700s and 1100-1400s, respectively. This same behavior is observed in Figure 49 for the power where maximum power production of 1000 W occurs during peak power demand. We also make note that during the cruising profile, the charging

power demand reaches 1000 W for only a short time because charging occurs for only a brief period during the climbing segment before entering into the lower power cursing segment.

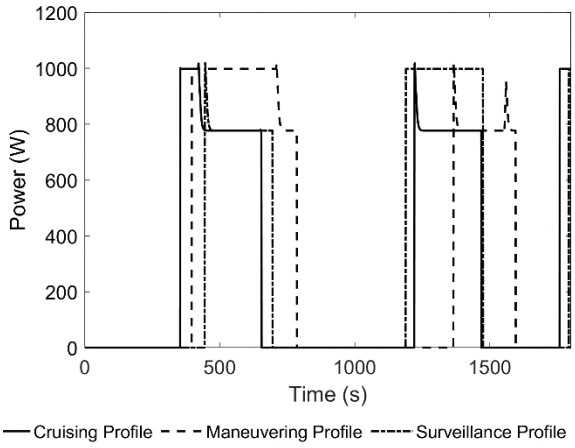

Figure 49. Baseline controller generator power

Analyzing the battery SOC (Figure 50), we see that initially, the SOC decreases at the same rate for each mission; however, once charging begins, the charging rate is for each profile. The maneuvering profile exhibits a longer charging duration, possibly because the climbing segment is the longest of all the missions, and higher flight speed is requested during the climb. This combination of factors can lead to a situation where the charging operation can be delayed until power demand drops. We also see the at the 1000 s point, the SOC for the surveillance profile has a sharp decrease, which corresponds to the aircraft beginning to enter the evasion phase where power demand is high.

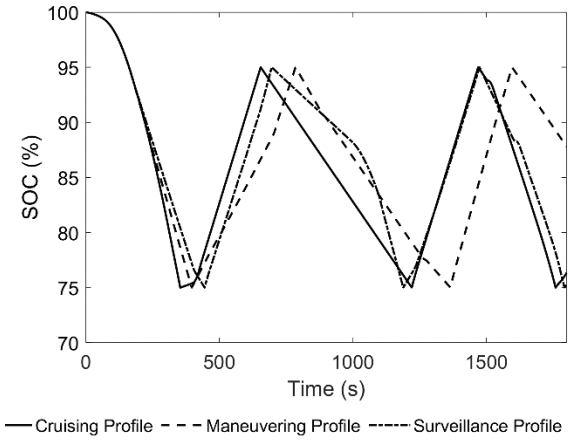

Figure 50. Baseline controller battery SOC

More importantly, the fuel consumption of the hybrid powertrain is one of the most critical aspects of the powertrain performance and is the main focus of each controller analyzed in this work. As shown in Figure 51, the baseline controller used 123 g to 90 g of fuel, with the maneuvering profile using the most fuel. The maneuvering profile possibly uses more fuel because of the extended climbing phase, which results in more fuel being used in the first 800s of flight.

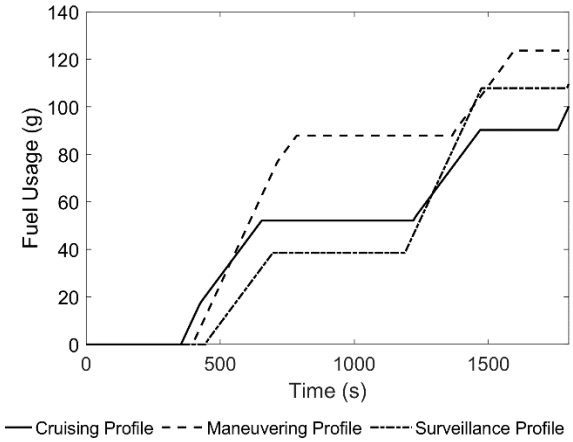

Figure 51. Baseline controller engine fuel consumption

5.3. IOL Control Results

The IOL controller produces roughly the same current as the baseline controller during charging, as shown in Figure 52. The current varies between 37 A to 42 A. However, we see that

at the 700s point, some oscillations exist, which are a result of the controller attempting to operate at the specified ideal operating line profile. These oscillations could be a direct result of the IOL line construction where the power or torque needed to generate power occurs in a range where the IOL line has sharp changes causing issues with the look-up tables used to define the line.

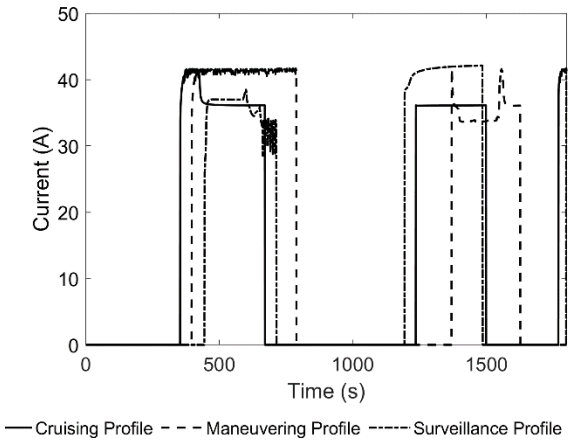

Figure 52. IOL controller generator current

The power profile for the maneuvering and surveillance profile has roughly the same levels of peak power production as observed for the baseline controller. However, one notable observation is that the IOL controller has more transient operation for the maneuvering profile around the 1300-1500s range (Figure 53). This range corresponds directly to a phase where the aircraft accelerates to a higher speed before entering into the last cursing segment of the mission. Thus these transient spikes correspond to the period where the aircraft is undergoing acceleration from 23 m/s to 30 m/s, thus causing power spikes in the generator power demand.

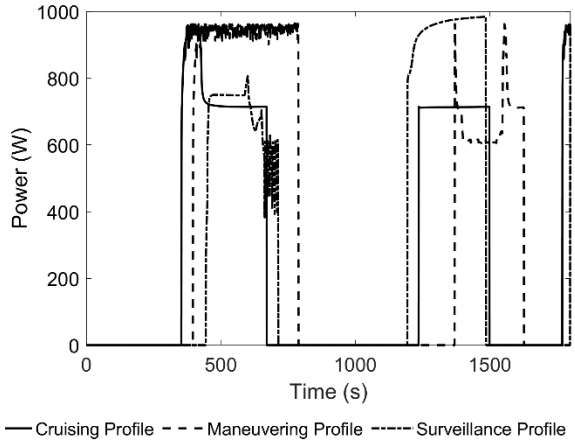

Figure 53. IOL controller generator power

For the IOL battery SOC (Figure 54), we see again that initially, the SOC decreases at the same rate for each mission; however, once charging beings, the profiles begin to diverge. This profile looks nearly identical to that of the baseline controller, where the maneuvering profile exhibits a longer charging because the climbing segment and the SOC for the surveillance profile have a sharp decrease at the 1000s point, which corresponds to the aircraft beginning to enter the evasion phase.

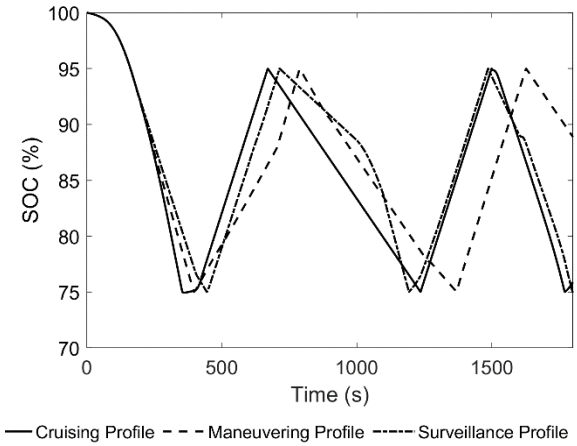

Figure 54. IOL controller battery SOC

Although the performance shown in Figure 52 -Figure 54 might seem very similar to what was observed in the baseline controller, slight differences exist. The most notable difference is

shown in Figure 55 of the fuel usage for the IOL controller. The IOL scheme used 82 g to 109 g of fuel across the three different missions, with the maneuvering profile using the most fuel. This higher fuel consumption for the maneuvering profile is again because of the more prolonged climbing phase used in the first 800s of flight resulting in more fuel consumption. We see that the IOL controller was able to reduce fuel consumption considerably when compared to the baseline controller. This shows the effectiveness of the IOL controller simply through the addition of the IOL line, which defines the most efficient line or region of operation.

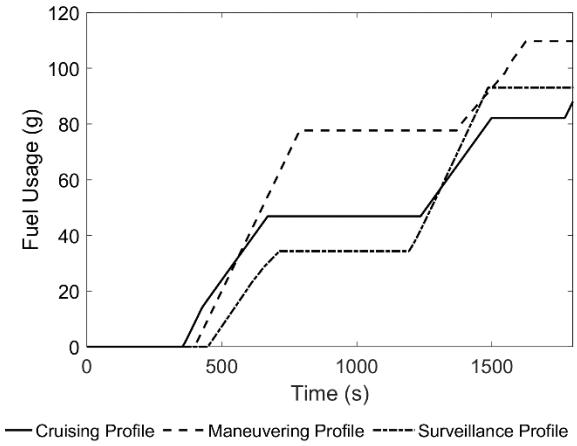

Figure 55. IOL controller engine fuel consumption

5.4. Fuzzy Logic Control Results

The FLC controller is able to consistently produce 40 A of current for each of the missions, which in comparison to the baseline and the IOL current generally was less for the cruising and surveillance profile at certain times. These results are possible due to the control having the ability to control more aspects of the powertrain function, thus controlling the generator power production better. However, we see a couple of current spikes occurring at the 700s and the 1500s point, which again are a result of transient behavior associated with the transition from charge sustaining to charge depletion mode, as shown in Figure 58, where the maximum SOC is reached.

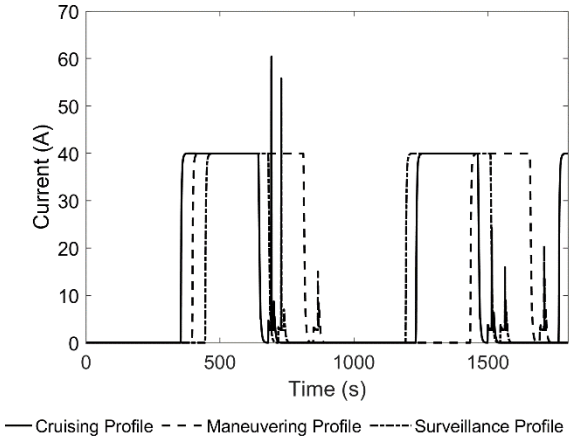

Figure 56. FLC controller generator current

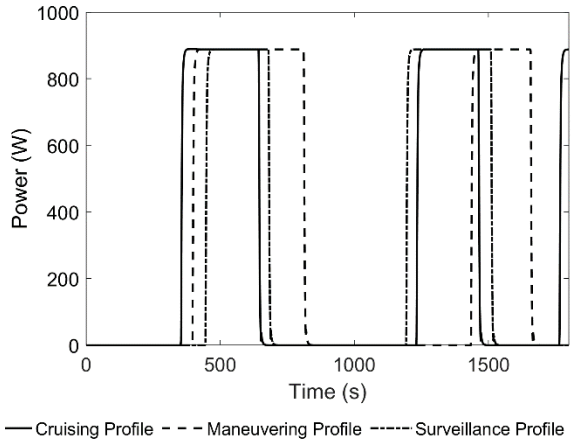

Figure 57. FLC controller generator power

The power profile for the fuzzy logic controller (Figure 57) is much lower than the IOL or the baseline controller. The FLC operates the engine at 888 W compared to the 956 W and 1000 W of power for the IOL and baseline controller, respectively. The FLC, because of its ability to use multi-valued logic and multiple input variables, can control the power production of the generator better.

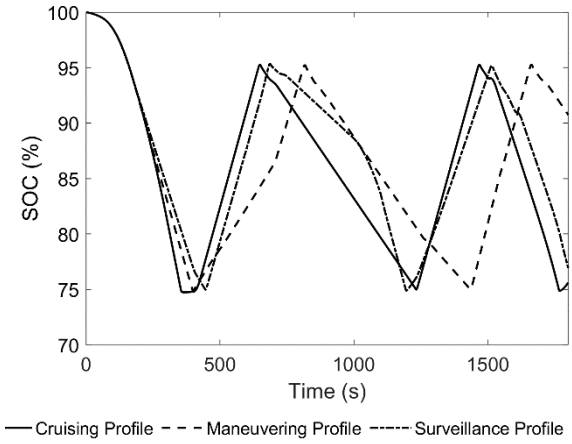

Figure 58. FLC controller battery SOC

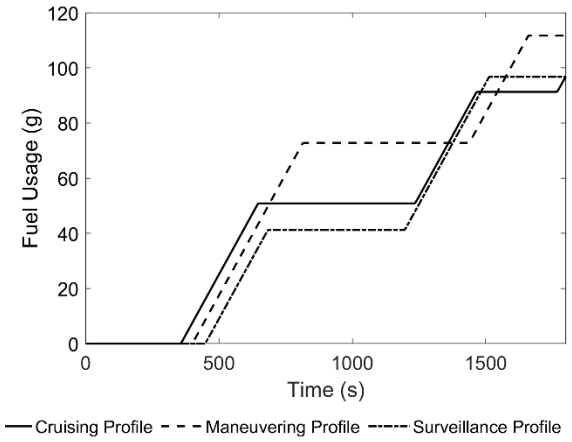

Figure 59. FLC controller engine fuel consumption

The battery SOC (Figure 58) for the fuzzy logic controller demonstrates again that initially, the SOC decreases at the same rate for each mission and then begin to diverge. This profile look shape is nearly identical to the results of the other previously mentioned controller; however, it is noticeable that the charging duration for the maneuvering and survalence mission is longer than the IOL and the baseline controller. This is due to the lower power production of the fuzzy logic controller compared to the IOL and the baseline controller.

The FLC scheme used 91 g to 111 g of fuel (Figure 59) among the three missions again with the maneuvering profile using the most fuel. The fuzzy logic controller manages to more

closely match the performance of the IOL controller, where total fuel consumption is similar. Thus the FLC results show that it could provide ample power for charging the batteries, albeit at longer charging times depending on the mission with comparable fuel consumption to the IOL controller. The next section aims to compare the fuel and BSFC performance of each controller in terms of the mission to determine which controller overall function better over each mission scenario.

5.5. Control Method Fuel Consumption Comparison

As discussed in previous chapters, fuel consumption is a vital performance parameter that demonstrates the efficiency of the controller. A control strategy that can efficiently operate the engine offers significant benefits for a hybrid powertrain. Ultimately the controller that provides the best performance can provide efficient operation in the majority of operating conditions. Thus the results in Figure 60 show that the IOL controller offers the least fuel consumption but not by much compared to the fuzzy logic controller in some scenarios. However, the baseline controller is by far the least efficient form of control for operating the engine efficiently for a series hybrid powertrain. In Figure 60a, the fuel consumption for the FLC and the baseline scheme are the same, while the IOL method has nearly a 12.5% difference. This trend, however, is very different for the maneuvering and the surveillance profile where the difference between the IOL and the FLC is much smaller. The difference in fuel consumption between the IOL and the FLC is only 1.8%, while the difference between the baseline is again nearly 12%, which is also the same difference between the IOL, FLC, and the baseline controller for the surveillance mission.

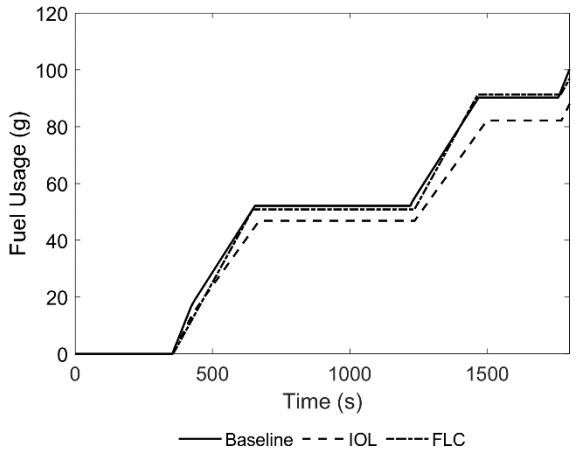

(a) Cruising mission

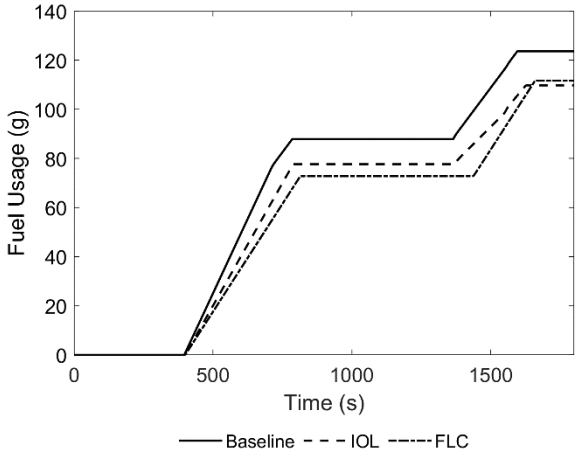

(b) Maneuvering mission

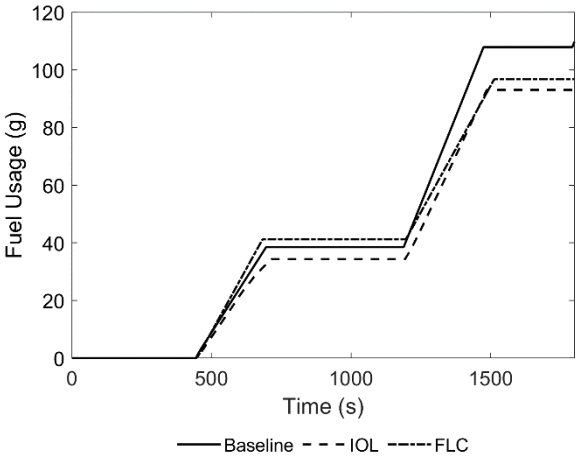

(c) Survalence Mission

Figure 60. Controller fuel consumption per flight mission

Thus one can conclude that the baseline controller uses approximately 12% more fuel than a controller that is more oriented in providing efficient engine operation. This is further shown in Table 5, where the fuel economy for each mission and each controller is shown. As shown in Table 5, the IOL method is generally more efficient. However, this efficiency results from the IOL and the results that one achieves are highly dependant on the accuracy of the data used to construct the IOL. Moreover, it might not be possible for the aircraft to achieve operation near the IOL because of environmental effects or other external factors that lower the engine efficiency.

Table 5. Controller fuel economy comparison

	Fuel Economy (g/km)		
Control Strategy	Cruising Profile	Maneuvering Profile	Surveillance Profile
Baseline	2.18	2.43	2.23
IOL	1.92	2.16	1.90
Fuzzy Logic	2.11	2.20	1.97

However, considering the design freedom of the FLC and how close the performance is to the IOL, it is possible that the rules and membership function used in this analysis are not optimal, and further refinement is possible, which could yield further fuel savings.

Chapter 6. Hardware Setup

To validate the performance results achieved in the powertrain system simulation, a physical hybrid powertrain testbed was constructed to test the control schemes. The physical system is composed of many of the same components in the powertrain model. However, to simplify the model, the actual components were not modeled identically to the physical system. The prop motor and generator are the same KDE 7215XF-135 BLDC motor, which is controlled by the KDE-UAS95HVC ESC, where the ESC for the generator functions as an inverter converting 3 phase AC power into DC power.

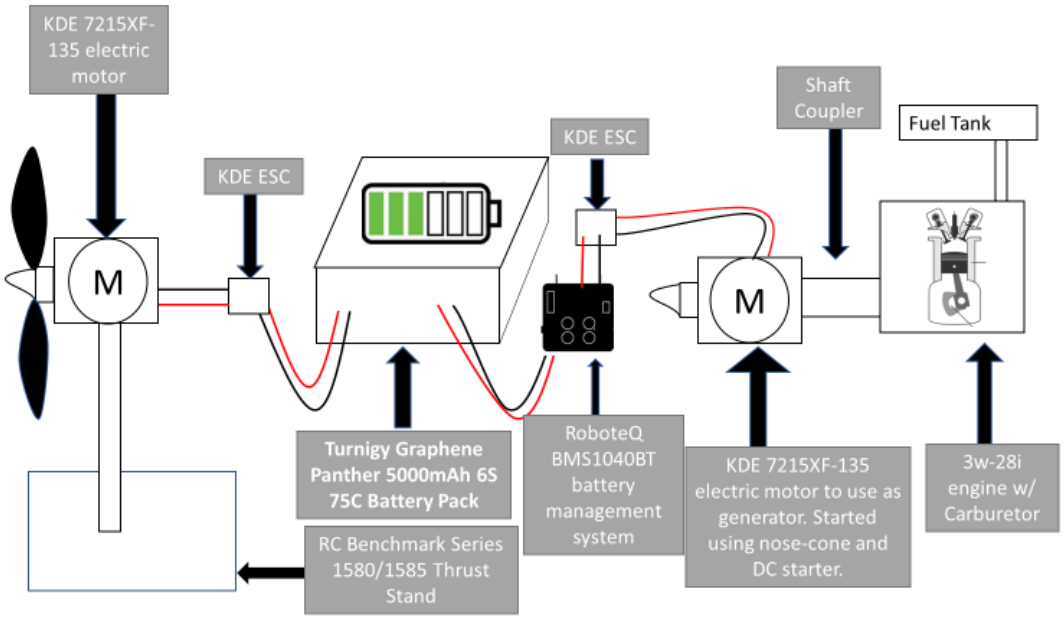

Figure 61. Hardware setup diagram

The prop motor is attached to an RC Benchmark series 1580 thrust stand and dynamometer, which uses load cells to measure the torque generated by the motor. The trust stand is capable of measuring thrust up to 1.5 kgf and 1.5 Nm of torque. An 18x6 Aerostar propeller connected to the prop motor generates the thrust for the system. The RC Benchmark testing program allows for logging of data such as prop motor torque, power, voltage, current, and speed in addition to propeller thrust generated. The ICE engine used is the 3W-28i, which is a carbureted 2-stroke

engine with a displacement of 28cc. Engine ignition is controlled by the 3W ignition control module, which uses the crank position signal to determine spark timing. The crank position sensor is composed of two magnets strategically placed on the engine crank snout, which is read by a magnetic pickup. The engine throttle is controlled via a small servo motor, and feedback control can be implemented to control the engine speed through the crank speed sensor and the throttle actuator. Engine starting is achieved using a nose cone adaptor connected to the rear of the generator and a common nose cone electric starter motor. However, in the future, engine starting can be accomplished directly using the generator as a motor to rotate the engine when requested. Lastly, the engine is connected to the generator motor via a flexible shaft coupler to form the gen-set.

The charging operation is triggered by the powertrain control when the SOC falls below the set value. The battery used in this system is a small hobby aircraft-grade Turnigy Graphene Panther 6s 22.2 V, 5 Ah LiPo battery, which is connected to a Roboteq 1040A BMS that manages the battery charging operations by balancing the voltage to each cell in addition to delivering power to the prop motor. This BMS unit also allows for the measurement of the charging and discharging current, battery load voltage, and the battery SOC. The powertrain components communicate through a National Instruments DAQ and a Labview interface. The LabVIEW interface also serves as the communication link between the powertrain controller in the Simulink environment. This allows for the necessary communication channels from the component and the powertrain controller to send information feedback between the components and the controller. The information is then processed by the controller to determine the necessary control actions.

A Labview interface was created to log and view powertrain performance data during the real-time simulation. This interface allows for viewing data for physical components: the motor,

engine, generator, propeller, and battery data, and displays data such as rotational speed, electrical power, thrust, motor torque, voltage, current, and battery SOC. The interface allows for viewing data for simulated components such as the aircraft, where data for flight speed, flight angle, and flight altitude. The LabVIEW application will also allow for direct control of the powertrain so that malfunctions and errors can be resolved or halted before damage to the hardware can occur and also allows for automatic limits to be set to protect the components.

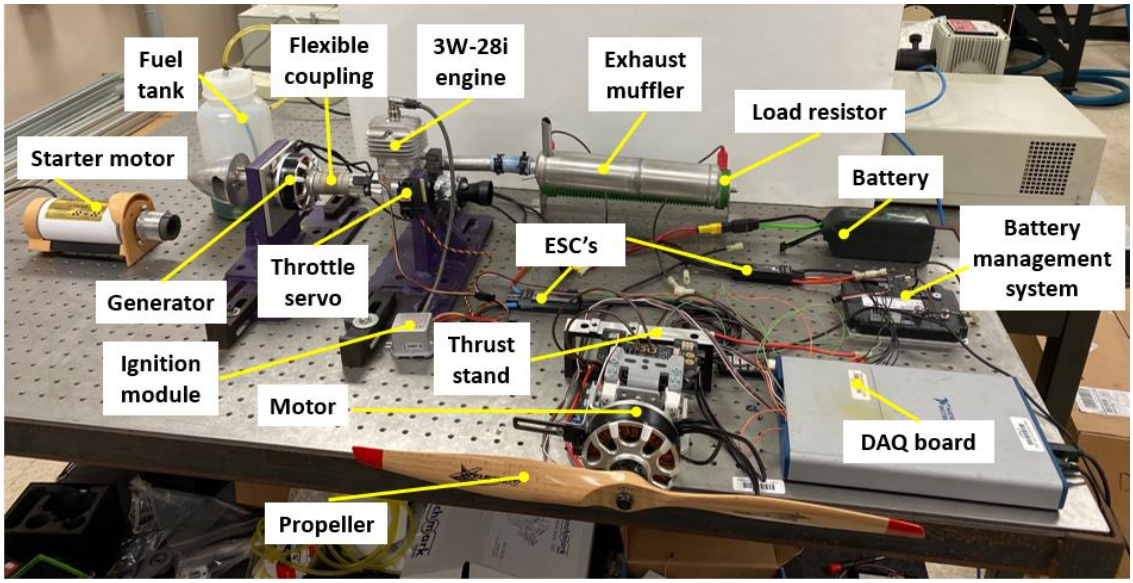

Figure 62. Physical testbed image

The series hybrid test stand (Figure 62) is necessary to validate all modeling aspects such as model accuracy, controller performance, and the development of new control schemes. This test stand can be used to verify model parameters to ensure that the model performance closely matches the physical hardware. This aspect of model accuracy is especially essential if higher fidelity models are implemented for the powertrain components by allowing for the use of physical test data to tune the component model performance. Controller performance tuning and validation is another important use for the testbed. The controllers developed in this work, such as the IOL and the fuzzy logic controller, can be refined for accuracy and efficacy. For example, the fuzzy logic controller implementation could be refined based upon which information is gathered from the

initial test of the controller performance. This information can then be used to modify the membership functions and rules to achieve the desired performance that is observed in the physical hardware test. The central goal of the physical testbed is to confirm that the controllers and models are accurately predicting the system performance and that the fuel consumption savings observed for the various mission simulations between the different controllers are possible.

Chapter 7. Conclusions

7.1. Concluding Remarks

Hybrid powertrains offer potential improvement in range and endurance performance, in addition to noise, fuel cost savings, and engine emissions in propulsion systems for unmanned aircraft. Unfortunately, the current understanding of the performance benefits specific to different hybrid powertrain configurations is lacking. Furthermore, the current understanding of benefits from powertrain hybridization for small unmanned aerial systems is lacking. This is primarily due to a lack of adequate consideration of the performance of individual powertrain components, with sufficient attention to a robust control strategy for the powertrain operation. This work aims to use a high-level powertrain system model for unmanned air systems to perform comparative performance analysis for different powertrain controllers tested using different mission profiles. The objective is to study integrated powertrain performance and evaluate the significance of utilizing an appropriate control strategy to minimize overall fuel consumption.

A system model of a series hybrid electric UAS was constructed, which incorporated detailed models of the powertrain components. Component models included measured performance maps such as those for the IC engine and models incorporating tuned input parameters obtained from hardware test data such as those for the battery, motor, and generator. Three different powertrain control strategies were employed, where two focused on efficient engine operation. The first controller named the baseline strategy, functioned as a power-follower form of control, generating the requested power without considering engine fuel consumption. Next, an ideal operating line (IOL) controller that optimizes engine fuel consumption is used to control the hybrid powertrain operation. The controller attempted to optimize engine fuel consumption by choosing engine operating points corresponding to generator power demand with the lowest brake specific fuel

consumption(BSFC). The IOL controller was aided in this process by a detailed engine map providing torque, power, and fuel consumption values measured for a typical engine used in unmanned air system. Lastly, a fuel efficiency-focused fuzzy logic controller was implemented to examine if further gains in fuel efficiency could be achieved by factoring in more variables of the powertrain operation.

Overall, the IOL strategy was shown to increase fuel efficiency over the baseline and fuzzy logic control strategy for a series hybrid powertrain configuration for all three mission profiles studied in this work. The IOL fuel savings were shown to range from 14 g to 16 g for a 30-minute duration mission profile when compared to the baseline controller. Also, the IOL generally has a 2g to 3g advantage over the fuzzy logic method with one exception where FLC used 10g more fuel for the cruising mission profile. These resulting fuel consumption values give an average improvement in fuel economy ranging from 12%-15% for the IOL and fuzzy logic scheme when compared to the baseline controller for specific missions. The results of this study show that the IOL configuration provides more fuel-efficient operation even over the FLC method. However, because of the flexibility of the FLC controller, further gains are possible. These further gains are apparent, considering that the performance is very close in two out of the three missions analyzed. The results produced by the FLC could see improvement through the refinement of both the membership functions used and the ruleset developed for the controller.

Aircraft hybrid powertrains are an emerging technology in the aerospace industry. In the scope of this work, hybrid UAVs could offer a tactical advantage for the armed forces in all uses cases such as surveillance, tactical, or strategic situations. Benefits such as increased range allow for the extension of the target region and the surveillance zone or increased endurance, allowing for a longer flight, thus increasing the effectiveness of UAV to complete a mission or multiple

mission before requiring refueling. Lastly, the rate of charging, which differs from one control scheme to another, as shown by the results, can affect mission readiness for the UAS. The mission for a UAS could be altered mid-flight due to unforeseen circumstances. The ability of the controller to charge the batteries to a point where the UAS system is prepared to accomplish any task presented is crucial. For the commercial industry, these same befits in increased range, and endurance could translate into reduced fuel cost leading to reduced air travel fees. Also, it is possible that hybrid aircraft could aid in reducing noise pollution from airports and during the flight, which makes the experience of air travel more tolerable. Considering that hybrid powertrains can operate in electric-only mode, commercial aircraft could reduce the noise created by jet engines during take-off and landing.

Design challenges do exist, and research and development continue in all aspects of the hybrid powertrain. Considering that this design problem is a multidisciplinary effort, significant work needs to be performed in developing more advanced designs ranging from motor technology to aircraft material. The main advancement needed is higher energy density batteries to increase the battery energy capacity so that battery weight can be reduced. The reduction of battery weight can alone provide significant gains in hybrid powertrain effectiveness. Also, current off-the-shelf small displacement engine could improve in fuel-efficiency through the use of fuel injection, which is better at controlling fuel usages in comparison to a carburetor. In addition, the development of higher efficiency engines at this scale could result in less fuel consumed during flight, and thus, less fuel is needed to travel the same distance. Lastly, improvements in aircraft materials could benefit hybrid and conventional aircraft. A lighter aircraft structure would benefit a hybrid powertrain because it would allow for the added weight of the hybrid powertrain to be

offset by the reduced weight of the airframe. Hybrid aircraft are still in the infancy stages; however, the future of hybrid electric flight is promising where a new age of flight is possible.

7.2. Future works

Future efforts focus on improvements in the controller logic and engine performance maps with higher resolution to ensure an optimal ideal operating line is found. Other tasks include the modeling of the more complex parallel and split power configurations and exploring other possible control methods for these powertrain configurations. Considering that literature has done ample research on parallel hybrid powertrain control, this is the next logical step. Moreover, further improvements in model accuracy could be gained by incorporating higher fidelity models for the aircraft, motors, and possibly the battery.

Furthermore, efforts in developing a hardware platform for testing hybrid powertrains will continue where the models and the control schemes can be tested for accuracy and effectiveness. This hardware testbed will allow for the continued improvement of the model accuracy and control development.

Lastly, work is currently in progress to incorporate a higher fidelity 3 degree of freedom (3 DOF) aircraft model developed by our collaborators at Southern University – Baton Rouge. This model will be used to analyze the effect of a more accurate aircraft model on the powertrain controller and overall model performance. Environmental wind effects will also be incorporated in this analysis to observe the effects on the power consumption of small aircraft.

References

[1] Sabri, M. F. ., Danapalasingam, K. A., and Rahmat, M. F. “A Review on Hybrid Electric Vehicles Architecture and Energy Management Strategies.” *Renewable and Sustainable Energy Reviews*, Vol. 53, 2016, pp. 1433–1442. https://doi.org/10.1016/j.rser.2015.09.036.

[2] Brelje, B. J., and Martins, J. R. R. A. “Electric, Hybrid, and Turboelectric Fixed-Wing Aircraft: A Review of Concepts, Models, and Design Approaches.” *Progress in Aerospace Sciences*, Vol. 104, 2019, pp. 1–19. https://doi.org/10.1016/j.paerosci.2018.06.004.

[3] Topham, G. Rolls-Royce Joins Race to Develop Electric Passenger Jets. *Guardian News and Media*. https://www.theguardian.com/business/2017/nov/28/rolls-royce-electric-passenger-jets-airbus-siemens-e-fan-x-hybrid-electric-plane-2020. Accessed Oct. 19, 2020.

[4] NASA Armstrong Fact Sheet: NASA X-57 Maxwell. *NASA*. https://www.nasa.gov/centers/armstrong/news/FactSheets/FS-109.html. Accessed Oct. 19, 2020.

[5] Project Kick-off Meeting of EU H2020 CENTRELINE Hosted by Bauhaus Luftfahrt. *Bauhaus Luftfahrt*. https://www.bauhaus-luftfahrt.net/en/press-media/news/project-kick-off-meeting-of-eu-h2020-centreline-hosted-by-bauhaus-luftfahrt/. Accessed Oct. 19, 2020.

[6] Future Flight-Boeing: 2014 Environment Report. *Boeing*. http://www.boeing.com/aboutus/environment/environment_report_14/2.3_future_flight.html. Accessed Oct. 19, 2020.

[7] Siemens. Electric Hybrid Drives for Aircraft. *Phys.org*. https://phys.org/news/2013-07-electric-hybrid-aircraft.html. Accessed Oct. 19, 2020.

[8] Zero-Emission Air Transport – First Flight of Four-Seat Passenger Aircraft HY4. *HY4*. http://hy4.org/zero-emission-air-transport-first-flight-of-four-seat-passenger-aircraft-hy4. Accessed Oct. 19, 2020.

[9] Morlin-Yron, S. The Plane That Runs on Hydrogen and Emits Only Water. *CNN*. https://www.cnn.com/travel/article/hy4-fuel-cell-plane/index.html. Accessed Oct. 19, 2020.

[10] Fahlstrom, P., and Gleason, T. Classes and Missions of UAVs. In *Introduction to UAV systems*, John Wiley & Sons, Chichester, 2012, pp. 17–31.

[11] Boeing Insitu ScanEagle Drones Sold to Malaysia, Indonesia, Philippines, Vietnam. *The Defense Post*. https://www.thedefensepost.com/2019/06/01/boeing-insitu-scaneagle-drones-malaysia-indonesia-philippines-vietnam/. Accessed Oct. 19, 2020.

[12] Thurber, M. Lycoming Engines Sees New Markets In UAS Segment. *Aviation International News*. https://www.ainonline.com/aviation-news/defense/2014-07-16/lycoming-engines-sees-new-markets-uas-segment. Accessed Oct. 19, 2020.

[13] Wu, G., Zhang, X., and Dong, Z. "Powertrain Architectures of Electrified Vehicles: Review, Classification and Comparison." *Journal of the Franklin Institute*, Vol. 352, No. 2, 2015, pp. 425–448. https://doi.org/10.1016/j.jfranklin.2014.04.018.

[14] Singh, K. V., Bansal, H. O., and Singh, D. "A Comprehensive Review on Hybrid Electric Vehicles: Architectures and Components." *Journal of Modern Transportation*, Vol. 27, No. 2, 2019, pp. 77–107. https://doi.org/10.1007/s40534-019-0184-3.

[15] Carey, S. B. *Increasing the Endurance and Payload Capacity of Unmanned Serial Vehicles with Thin-Film Photovoltaics*. Thesis. Naval Postgraduate School: Monterey, California:, 2014.

[16] Olsen, J., and Page, J. R. "Hybrid Powertrain for Light Aircraft." *International Journal of Sustainable Aviation*, Vol. 1, No. 1, 2014, p. 85. https://doi.org/10.1504/IJSA.2014.062871.

[17] Menon, S. K. *Performance Measurement and Scaling in Small Internal Combustion Engines*. Dissertation. University of Maryland, College Park, 2006.

[18] Gong, Z., and Yang, Y. "Recent Advances in the Research of Polyanion-Type Cathode Materials for Li-Ion Batteries." *Energy & Environmental Science*, Vol. 4, No. 9, 2011, p. 3223. https://doi.org/10.1039/c0ee00713g.

[19] Soloveichik, G. L. "Battery Technologies for Large-Scale Stationary Energy Storage." *Annual Review of Chemical and Biomolecular Engineering*, Vol. 2, No. 1, 2011, pp. 503–527. https://doi.org/10.1146/annurev-chembioeng-061010-114116.

[20] Nazar, L. F., Cuisinier, M., and Pang, Q. "Lithium-Sulfur Batteries." *Materials Research Society Bulletin*, Vol. 39, No. 5, 2014, pp. 436–442. https://doi.org/10.1557/mrs.2014.86.

[21] Mikhaylik, Y., Kovalev, I., Xu, J., and Schock, R. "Rechargeable Li-S Battery with Specific Energy 350 Wh/Kg and Specific Power 3000 W/Kg." *Electrochemical Society Meeting Abstracts*, 2008, pp. 1–2. https://doi.org/10.1149/MA2008-01/5/112.

[22] Girishkumar, G., McCloskey, B., Luntz, A. C., Swanson, S., and Wilcke, W. "Lithium-Air Battery: Promise and Challenges." *Journal of Physical Chemistry Letters*, Vol. 1, No. 14, 2010, pp. 2193–2203. https://doi.org/10.1021/jz1005384.

[23] Pipistrel ALPHA Electro - The First LSA Certified Electric Aircraft. Pipistrel USA. *Pipistrel*. https://www.pipistrel-usa.com/alpha-electro/. Accessed Oct. 19, 2020.

[24] Schömann, J. *Hybrid-Electric Propulsion Systems for Small Unmanned Aircraft*. Dissertation. Technical University of Munich, 2014.

[25] Brown, S. P. *Design and Optimization of a 1 KW Hybrid Powertrain for Unmanned Aerial Vehicles*. Thesis. Oregon State University, 2017.

[26] Voskuijl, M., van Bogaert, J., and Rao, A. G. "Analysis and Design of Hybrid Electric Regional Turboprop Aircraft." *Council of European Aerospace Societies Aeronautical Journal*, Vol. 9, No. 1, 2017, pp. 15–25. https://doi.org/10.1007/s13272-017-0272-1.

[27] Menon, S., and Cadou, C. P. "Scaling of Miniature Piston-Engine Performance, Part 1: Overall Engine Performance." *Journal of Propulsion and Power*, Vol. 29, No. 4, 2013, pp. 774–787. https://doi.org/10.2514/1.B34638.

[28] Rowton, A. K. *Measuring Scaling Effects in Small Two-Stroke Internal Combustion Engines*. Thesis. Air Force Institute of Technology, 2014.

[29] Silva, H. L. *Hybrid-Electric Aircraft: Conceptual Design, Structural and Aeroelastic Analyses*. Thesis. Federal University of Uberlândia, 2017.

[30] Isikveren, A. T., Kaiser, S., Pornet, C., and Vratny, P. C. "Pre-Design Strategies and Sizing Techniques for Dual-Energy Aircraft." *Aircraft Engineering and Aerospace Technology*, Vol. 86, No. 6, 2014, pp. 525–542. https://doi.org/10.1108/AEAT-08-2014-0122.

[31] Sliwinski, J., Gardi, A., Marino, M., and Sabatini, R. "Hybrid-Electric Propulsion Integration in Unmanned Aircraft." *Energy*, Vol. 140, No. July, 2017, pp. 1407–1416. https://doi.org/10.1016/j.energy.2017.05.183.

[32] Donateo, T., and Ficarella, A. "Designing a Hybrid Electric Powertrain for an Unmanned Aircraft with a Commercial Optimization Software." *Society of Automotive Engineers International Journal of Aerospace*, Vol. 10, No. 1, 2017. https://doi.org/10.4271/2017-01-9000.

[33] Hiserote, R. M. *Analysis of Hybrid-Electric Propulsion System Designs for Small Unmanned Aircraft Systems*. Thesis. Air force institute of technology. Wright-patterson air force Base, Ohio, 2010.

[34] Rotramel, T. A. *Optimization of Hybrid-Electric Propulsion Systems for Small Remotely-Piloted Aircraft*. Thesis. Air force institute of technology. Wright-patterson air force Base, Ohio, 2011.

[35] Xie, Y., Savvaris, A., and Tsourdos, A. "Sizing of Hybrid Electric Propulsion System for Retrofitting a Mid-Scale Aircraft Using Non-Dominated Sorting Genetic Algorithm." *Aerospace Science and Technology*, Vols. 82–83, 2018, pp. 323–333. https://doi.org/10.1016/j.ast.2018.09.022.

[36] Sgueglia, A., Schmollgruber, P., Bartoli, N., Benard, E., Morlier, J., Jasa, J., Martins, J. R. R. A., Hwang, J. T., and Gray, J. S. "Multidisciplinary Design Optimization Framework with Coupled Derivative Computation for Hybrid Aircraft." *Journal of Aircraft*, Vol. 57, No. 4, 2020, pp. 715–729. https://doi.org/10.2514/1.C035509.

[37] Sinibaldi, G., and Marino, L. “Experimental Analysis on the Noise of Propellers for Small UAV.” *Applied Acoustics*, Vol. 74, No. 1, 2013, pp. 79–88. https://doi.org/10.1016/j.apacoust.2012.06.011.

[38] Enang, W., and Bannister, C. “Modelling and Control of Hybrid Electric Vehicles (A Comprehensive Review).” *Renewable and Sustainable Energy Reviews*, Vol. 74, 2017, pp. 1210–1239. https://doi.org/10.1016/j.rser.2017.01.075.

[39] Meisel, J., Shabbir, W., and Evangelou, S. A. “A Practical Control Methodology for Parallel Plug-in Hybrid Electric Vehicle Powertrains.” *2013 9th IEEE Vehicle Power and Propulsion Conference*, 2013. https://doi.org/10.1109/VPPC.2013.6671659.

[40] Gao, J., Sun, F., He, H., Zhu, G. G., and Strangas, E. G. “A Comparative Study of Supervisory Control Strategies for a Series Hybrid Electric Vehicle.” *Asia-Pacific Power and Energy Engineering Conference*, 2009. https://doi.org/10.1109/APPEEC.2009.4918038.

[41] Lee, B., Park, P., Kim, C., Yang, S., and Ahn, S. “Power Managements of a Hybrid Electric Propulsion System for UAVs.” *Journal of Mechanical Science and Technology*, Vol. 26, No. 8, 2012, pp. 2291–2299. https://doi.org/10.1007/s12206-012-0601-6.

[42] Barsali, S., Miulli, C., and Possenti, A. “A Control Strategy to Minimize Fuel Consumption of Series Hybrid Electric Vehicles.” *IEEE Transactions on Energy Conversion*, Vol. 19, No. 1, 2004, pp. 187–195. https://doi.org/10.1109/TEC.2003.821862.

[43] Machado, L., Matlock, J., and Suleman, A. “Experimental Evaluation of a Hybrid Electric Propulsion System for Small UAVs.” *Aircraft Engineering and Aerospace Technology*, Vol. 92, No. 5, 2019, pp. 727–736. https://doi.org/10.1108/AEAT-06-2019-0120.

[44] Hung, J. Y. C., and Gonzalez, L. F. “Design, Simulation and Analysis of a Parallel Hybrid Electric Propulsion System for Unmanned Aerial Vehicles.” *28th Congress of the International Council of the Aeronautical Sciences 2012, ICAS 2012*, Vol. 4, 2012, pp. 2655–2661.

[45] Xie, Y., Savvaris, A., Tsourdos, A., Laycock, J., and Farmer, A. “Modelling and Control of a Hybrid Electric Propulsion System for Unmanned Aerial Vehicles.” *IEEE Aerospace Conference Proceedings*, 2018. https://doi.org/10.1109/AERO.2018.8396436.

[46] Gao, J. P., Zhu, G. M. G., Strangas, E. G., and Sun, F. C. “Equivalent Fuel Consumption Optimal Control of a Series Hybrid Electric Vehicle.” *Proceedings of the Institution of Mechanical Engineers, Part D: Journal of Automobile Engineering*, Vol. 223, No. 8, 2009, pp. 1003–1018. https://doi.org/10.1243/09544070JAUTO1074.

[47] Harmon, F. G., Frank, A. A., and Joshi, S. S. “The Control of a Parallel Hybrid-Electric Propulsion System for a Small Unmanned Aerial Vehicle Using a CMAC Neural Network.” *Neural Networks*, Vol. 18, Nos. 5–6, 2005, pp. 772–780. https://doi.org/10.1016/j.neunet.2005.06.030.

[48] Yan, F., Wang, J., and Huang, K. “Hybrid Electric Vehicle Model Predictive Control Torque-Split Strategy Incorporating Engine Transient Characteristics.” *IEEE Transactions on Vehicular Technology*, Vol. 61, No. 6, 2012, pp. 2458–2467. https://doi.org/10.1109/TVT.2012.2197767.

[49] Liu, X., Wu, Y., and Duan, J. “Power Split Control Strategy for a Series Hybrid Electric Vehicle Using Fuzzy Logic.” *International Conference on Automation and Logistics*, 2008, pp. 481–486. https://doi.org/10.1109/ICAL.2008.4636199.

[50] Chen, Z., Zhang, X., and Mi, C. C. “Slide Mode and Fuzzy Logic Based Powertrain Controller for the Energy Management and Battery Lifetime Extension of Series Hybrid Electric Vehicles.” *Journal of Asian Electric Vehicles*, Vol. 8, No. 2, 2010, pp. 1425–1432. https://doi.org/10.4130/jaev.8.1425.

[51] Assadian, F., Mohan, G., and Longo, S. “Comparative Analysis of Forward-Facing Models vs Backward-Facing Models in Powertrain Component Sizing.” *Hybrid and Electric Vehicles Conference 2013*, 2013. https://doi.org/10.1049/cp.2013.1920.

[52] Chau, K. T., Li, W. L., and Lee, C. H. T. “Challenges and Opportunities of Electric Machines for Renewable Energy (Invited Paper).” *Progress In Electromagnetics Research B*, No. 42, 2012, pp. 45–74. https://doi.org/10.2528/PIERB12052001.

[53] Nise, N. S. Modeling in the Frequency Domain. In *Control Systems Engineering*, John Wiley & Sons, New York, 2015, p. 78.

[54] Baldursson, S. *BLDC Motor Modelling and Control – A Matlab®/Simulink® Implementation*. Thesis. Chalmers University of Technology, 2005.

[55] Saidani, F., Hutter, F. X., Scurtu, R.-G., Braunwarth, W., and Burghartz, J. N. “Lithium-Ion Battery Models: A Comparative Study and a Model-Based Powerline Communication.” *Advances in Radio Science*, Vol. 15, 2017, pp. 83–91. https://doi.org/10.5194/ars-15-83-2017.

[56] Barcellona, S., and Piegari, L. “Lithium Ion Battery Models and Parameter Identification Techniques.” *Energies*, Vol. 10, No. 12, 2017. https://doi.org/10.3390/en10122007.

[57] Si Li, and Ximing Cheng. “A Comparative Study on RC Models of Lithium-Ion Battery.” *2014 IEEE Conference and Expo Transportation Electrification Asia-Pacific*, 2014. https://doi.org/10.1109/ITEC-AP.2014.6940818.

[58] He, H., Xiong, R., and Fan, J. “Evaluation of Lithium-Ion Battery Equivalent Circuit Models for State of Charge Estimation by an Experimental Approach.” *Energies*, Vol. 4, No. 4, 2011, pp. 582–598. https://doi.org/10.3390/en4040582.

[59] Liu, G., Lu, L., Fu, H., Hua, J., Li, J., Ouyang, M., Wang, Y., Xue, S., and Chen, P. “A Comparative Study of Equivalent Circuit Models and Enhanced Equivalent Circuit Models of Lithium-Ion Batteries with Different Model Structures.” *2014 IEEE Conference*

and Expo Transportation Electrification Asia-Pacific, 2014. https://doi.org/10.1109/ITEC-AP.2014.6940946.

[60] Ahmed, R., Gazzarri, J., Onori, S., Habibi, S., Jackey, R., Rzemien, K., Tjong, J., and Lesage, J. "Model-Based Parameter Identification of Healthy and Aged Li-Ion Batteries for Electric Vehicle Applications." *SAE International Journal of Alternative Powertrains*, Vol. 4, No. 2, 2015, pp. 233–247. https://doi.org/10.4271/2015-01-0252.

[61] Liao, C., Li, H., and Wang, L. "A Dynamic Equivalent Circuit Model of LiFePO4 Cathode Material for Lithium Ion Batteries on Hybrid Electric Vehicles." *5th IEEE Vehicle Power and Propulsion Conference*, 2009. https://doi.org/10.1109/VPPC.2009.5289681.

[62] Yao, L. W., Aziz, J. A., Kong, P. Y., and Idris, N. R. N. "Modeling of Lithium-Ion Battery Using MATLAB/Simulink." *IECON 2013 - 39th Annual Conference of the IEEE Industrial Electronics Society*, 2013. https://doi.org/10.1109/IECON.2013.6699393.

[63] Zhao, S., and Howey, D. A. "Global Sensitivity Analysis of Battery Equivalent Circuit Model Parameters." *2016 IEEE Vehicle Power and Propulsion Conference*, 2016. https://doi.org/10.1109/VPPC.2016.7791696.

[64] Meng, H., Wang, L., Han, Z., and Lei, S. "Simulation of Engine Power Based on Mean Value Model." *International Organization of Scientific Research Journal of Engineering*, Vol. 3, No. 10, 2013, pp. 24–27. https://doi.org/10.9790/3021-031022427.

[65] Powell, J. D. "A Review of IC Engine Models for Control System Design." *International Federation of Automatic Control Proceedings Volumes*, Vol. 20, No. 5, 1987, pp. 235–240. https://doi.org/10.1016/s1474-6670(17)55378-1.

[66] Roskam, J., and Lan, C.-T. E. Equations of Motion. In *Airplane aerodynamics and performance*, DARcorporation, Lawrence, 1997, p. 374.

[67] Performance Data. *APC Propeller*. https://www.apcprop.com/technical-information/performance-data/. Accessed Oct. 19, 2020.

[68] Hung, J. Y., and Gonzalez, L. F. "On Parallel Hybrid-Electric Propulsion System for Unmanned Aerial Vehicles." *Progress in Aerospace Sciences*, Vol. 51, 2012, pp. 1–17. https://doi.org/10.1016/j.paerosci.2011.12.001.

Vita

Darren was born and raised in New Orleans, Louisiana, and later went on to receive his Bachelor of Science in Mechanical Engineering with a Minor in Aerospace Engineering from LSU in May 2018. Following graduation, he returned to. LSU to pursue his Master's Degree in Mechanical Engineering in August 2018. He began his graduate studies under the guidance of Dr. Shyam Menon in the Energy and Propulsion Laboratory on a new project focusing on hybrid-electric powertrains for unmanned aerial systems. Following his graduation in December 2020, Darren hopes to pursue a career in the aerospace industry where he can use his knowledge gained on hybrid aircraft technology to aid in developing future aircraft powertrains.